The Discrete Nonlinear Schrödinger Equation

Mathematical Analysis, Numerical Computations and Physical Perspectives

Bearbeitet von
Panayotis G. Kevrekidis

schnell und portofrei erhältlich bei

Chapter 2
The One-Dimensional Case

We now focus on the analysis of the one-dimensional DNLS equation of the form

$$i\dot{u}_n = -\epsilon \left(u_{n+1} + u_{n-1} - 2u_n \right) + \beta |u_n|^2 u_n. \tag{2.1}$$

(In the above form of Eq. (2.1), one of ϵ and β can be scaled out; e.g., β can be scaled out up to a sign by $u \rightarrow u\sqrt{|\beta|}$) Note that in the next few chapters we will be considering the focusing (attractive interaction in BEC) case of $\beta < 0$; the defocusing nonlinearity of $\beta > 0$ will be treated in a separate chapter. Our analysis in both this and in the following chapters will revolve around fundamental and excited state solutions of the equation, their stability, and dynamics. Perhaps the most fundamental among these is the single-pulse solitary wave that we now turn to.

2.1 Single-Pulse Solitary Waves

2.1.1 The Continuum Approach

2.1.1.1 General Properties of the Continuum Problem

We start by considering such pulses in the continuum limit. Given the opportunity, we also present here an interlude with some fundamental features of the one-dimensional continuum NLS equation of the general form

$$iu_t = -u_{xx} - |u|^{2\sigma} u \tag{2.2}$$

(where the subscript x, t denote partial derivatives with respect to the corresponding variable). For more details, the interested reader is referred to [1].

Equation (2.2) is a Hamiltonian system, but with infinite degrees of freedom (i.e., a "field theory"). As such, we expect that it will have a Lagrangian and a Hamiltonian *density*. Indeed, the Lagrangian density for the model is

$$\mathcal{L} = \frac{i}{2} \left(u^\star u_t - u u_t^\star \right) - |u_x|^2 + \frac{1}{\sigma + 1} |u|^{2\sigma + 2}. \tag{2.3}$$

Then, the corresponding partial differential equation (in particular, Eq. (2.2) in this case) is derived as the Euler–Lagrange equation of the field theory [1] according to

$$0 = \frac{\delta L}{\delta u} = \frac{\partial \mathcal{L}}{\partial u} - \partial_x \left(\frac{\partial \mathcal{L}}{\partial u_x} \right) - \partial_t \left(\frac{\partial \mathcal{L}}{\partial u_t} \right). \tag{2.4}$$

where $\delta L / \delta u$ symbolizes the Fréchet derivative [2] of the Lagrangian $L = \int \mathcal{L} dx$.

It can also be shown that if the action $S = \int L dt = \int \mathcal{L} dx dt$ is invariant under a transformation $x \to x + \delta x$, $t \to t + \delta t$ and $u \to u + \delta u$, then the quantity

$$I = \int dx \left[\frac{\partial \mathcal{L}}{\partial u_t} (u_t \delta t + u_x \delta x - \delta u) + C.C. - \mathcal{L} \delta t \right] \tag{2.5}$$

is conserved. This is the celebrated Noether theorem. Its proof requires the use of calculus of variations and we omit it here (the interested reader can find a detailed derivation in Sect. 2.2 of [1]).

For the particular Hamiltonian system of interest here, we have the following invariances (and corresponding conservation laws):

- if we use the transformation $u \to v = u e^{is}$ where s is space and time independent, then the equation for v is the same as the one for u. Hence there is a phase degeneracy/invariance in the system. The generator of the corresponding invariance is found as $v \approx u + \delta u$, with $\delta u = isu$ (the leading order expansion of the above mentioned exponential phase factor). Hence, using $\delta u = isu$ and $\delta x = \delta t = 0$, we obtain that

$$P = ||u||_{L^2}^2 = \int |u|^2 dx \tag{2.6}$$

  is conserved. This states that the (squared) L^2 norm is conserved by the dynamics of Eq. (2.2). This has a meaningful physical interpretation, e.g., in optics or BEC since in the former it states that the power of the beam is conserved, while in the latter it denotes the physically relevant conservation of the number of atoms in the condensate. This invariance is often referred to as the phase or gauge invariance of the NLS.
- Spatial translation $x \to x + \delta x$ also leaves Eq. (2.2) invariant. If we use $\delta t = \delta u = 0$ in Eq. (2.5), we obtain the conservation of linear momentum (just as in low-dimensional Hamiltonian systems of classical mechanics) of the form

$$M = i \int \left(u u_x^{\star} - u^{\star} u_x \right) dx. \tag{2.7}$$

Hence, translational invariance results in momentum conservation.

- Finally, time translation $t \to t + \delta t$ also leaves the dynamical equation invariant, hence using $\delta x = \delta u = 0$ in Eq. (2.5) results in the conservation of the Hamiltonian (i.e., the energy) of the system

$$H = \int \left(|u_x|^2 - \frac{1}{2\sigma + 2} |u|^{\sigma+1} \right) dx. \tag{2.8}$$

The integrand of Eq. (2.8) then represents the Hamiltonian density of the system. One can then restate the problem in the Hamiltonian (as opposed to the Lagrangian) formulation by means of Hamilton's equations and/or using the structure of the Poisson brackets, e.g.,

$$i u_t = \frac{\delta H}{\delta u^\star} = \{H, u\}, \tag{2.9}$$

where the standard Poisson bracket has been used.

These are general symmetries/invariances that are present for any value of σ. We now turn to the specific, the so-called integrable case of $\sigma = 1$. The integrability of this particular case means that apart from these three above defined integrals of motion, there are infinitely many others. The unusual feature of such an integrable nonlinear partial differential equation (PDE) is that once the initial data is prescribed, we can solve the PDE for all times [3]. The nonlinear wave solutions to such PDEs are often referred to as solitons, because they are solitary coherent structures (i.e., nonlinear waves) which emerge unscathed from their interaction with other such structures.

Here we focus on the standing wave solitons of the $\sigma = 1$ case, as the main solution of the solitary pulse type. Our exposition will highlight the features of this main "building block" of the NLS equation and will show how it is modified in the presence of the non-integrable perturbation imposed by discreteness.

Such standing wave solutions can be straightforwardly obtained in an explicit form

$$u = (2\Lambda)^{1/2} \text{sech}(\Lambda^{1/2}(x - ct - x_0)) e^{i\left(\frac{c}{2}x + (\Lambda - \frac{c^2}{4})t\right)}, \tag{2.10}$$

where Λ is the frequency of the wave, x_0 the initial position of its center, and c its speed. Since, there is an additional Galilean invariance, that allows us to boost a given solution to any given speed c, we will mostly focus on solutions with $c = 0$ hereafter. (Note, however, that discreteness does not preserve this invariance, hence the issue of traveling becomes an especially delicate one in the discrete case, as discussed in Part II.) These are often referred to as standing waves or occasionally as breathers (because of their periodicity in time and exponential localization in space).

Naturally, once such solutions are identified, the immediate next question concerns their stability. This can be identified at a first (but still particularly useful) step by means of linear stability analysis. Using the ansatz

$$u = e^{i\Lambda t} \left(u_0(x) + \varepsilon(v + iw)\right) \tag{2.11}$$

in Eq. (2.2), where $u_0(x) = (2\Lambda)^{1/2}\text{sech}(\Lambda^{1/2}(x - x_0))$, one obtains the linear stability equations by the $O(\varepsilon)$ expansion. It can be easily seen that the $O(1)$ equation is, by construction, identically satisfied (it is the equation satisfied by the solitary wave). The $O(\varepsilon)$ equations read as follows:

$$v_t = L_- w = \left(-\Delta + \Lambda - u_0^{2\sigma}\right) w, \tag{2.12}$$

$$w_t = -L_+ v = -\left(-\Delta + \Lambda - (2\sigma + 1)u_0^{2\sigma}\right) v. \tag{2.13}$$

In Eqs. (2.12) and (2.13), Δ denotes the second spatial derivative (per its natural higher dimensional generalization, namely the Laplacian). Note that we give the general form of the linear stability problem, even though for the time being we are interested in the particular case of $\sigma = 1$. Separating space and time variables for the solutions of the resulting equations (2.12) and (2.13) as $v(x, t) = e^{\lambda t}\tilde{v}(x)$ and $w(x, t) = e^{\lambda t}\tilde{w}(x)$, we obtain the eigenvalue problem in the form

$$\lambda^2 \tilde{v} = -L_- L_+ \tilde{v} \tag{2.14}$$

and similarly $\lambda^2 \tilde{w} = -L_+ L_- \tilde{w}$.

The invariances of the original equation are now mirrored in the zero eigenvalues of the linearization problem of Eq. (2.14). In particular, it is easy to check that for any solution of the form $u = e^{i\Lambda t}u_0(x)$, the spatial derivative du_0/dx corresponds to an eigenvector with a pair of zero eigenvalues since $L_+ du_0/dx = 0$. Similarly, the phase invariance leads to another pair of zero eigenvalues since $L_- u_0 = 0$. Hence, the linearization around the pulse-like soliton solutions of Eq. (2.10) will contain four eigenvalues at $\lambda = 0$. The algebraic multiplicity of the eigenvalues at the origin is four, but the geometric multiplicity is two. That is, each of the eigenvalues has an eigenvector and a *generalized* eigenvector associated with it. For example, the phase invariance has a generalized eigenvector $v = \partial u_0/\partial\Lambda$ [4, 5], satisfying $L_+ v = -u_0$. Similarly, there is a generalized eigenvector of translation proportional to $(x - x_0)u_0$ [4].

Furthermore, the linearization problem of Eqs. (2.12) and (2.13) will contain continuous spectrum. The latter consists of small amplitude, extended in space, plane wave eigenfunctions of the form $v + iw \propto e^{i(kx-\omega t)}$ (see [4] for their precise functional form). These satisfy the linear dispersion relation (upon substitution into the above equations) of the form

$$\omega^2 = -\lambda^2 = \pm\left(\Lambda + k^2\right). \tag{2.15}$$

Hence, in this case, the spectral plane (λ_r, λ_i) of the eigenvalues $\lambda = \lambda_r + i\lambda_i$ of the linearization around a soliton of the top panel of Fig. 2.1 will have a form such as the one given in the bottom panel of Fig. 2.1.

Fig. 2.1 The *top panel* shows the continuum soliton of the NLS equation for $\Lambda = 1$. The *bottom panel* shows the corresponding spectral plane of eigenvalues (λ_r, λ_i) in this integrable case. Four eigenvalues are at $\lambda = 0$ due to the invariances (see text) and the rest reside in the continuous spectrum whose band edge is at $\lambda = \pm\Lambda i$
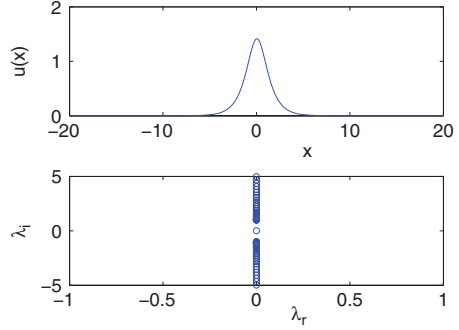
2.1.1.2 From Continuum to Discrete

The most straightforward discretization of the NLS equation

$$i\dot{u}_n = -\epsilon\Delta_2 u_n + \beta|u_n|^{2\sigma}u_n, \tag{2.16}$$

where $\epsilon = 1/h^2$, where h plays the role of the discrete lattice spacing and $\Delta_2 u_n = u_{n+1} + u_{n-1} - 2u_n$ is the discrete Laplacian with unit spacing. The DNLS model is also Hamiltonian with

$$H_{DNLS} = -\sum_{n=-\infty}^{\infty}\left[\epsilon|u_n - u_{n-1}|^2 + \frac{\beta}{\sigma+1}|u_n|^{2\sigma+2}\right] \tag{2.17}$$

and can be derived from H_{DNLS} as

$$\dot{u}_n = \{H_{DNLS}, u_n\}, \tag{2.18}$$

using the Poisson brackets

$$\{u_m, u_n^\star\} = i\delta_{m,n}, \quad \{u_m, u_n\} = \{u_m^\star, u_n^\star\} = 0. \tag{2.19}$$

As we indicated above, the case of $\sigma = 1$ is integrable in the continuum limit. In the discrete case, the above-mentioned DNLS is a non-integrable discretization of the continuum model. On the other hand, however, there does exist an integrable discretization, namely the so-called Ablowitz–Ladik (AL-NLS) discretization of the NLS equation [6, 7]

$$i\dot{u}_n = -\epsilon\Delta_2 u_n + \frac{\beta}{2}(u_{n+1} + u_{n-1})|u_n|^2 \tag{2.20}$$

with similar notation as used in Eq. (2.16). In the case of the AL-NLS, the Hamiltonian is of the form

$$H_{AL\text{-}NLS} = -\sum_{n=-\infty}^{\infty}\left[\epsilon|u_n - u_{n-1}|^2 + \frac{1}{\beta}\ln\left(1 + \beta|u_n|^2\right)\right]. \qquad (2.21)$$

The AL-NLS equation is derived from $H_{AL\text{-}NLS}$ using the non-standard Poisson brackets

$$\{u_m, u_n^{\star}\} = i\delta_{m,n}(1 + \beta|u_n|^2), \quad \{u_m, u_n\} = \{u_m^{\star}, u_n^{\star}\} = 0. \qquad (2.22)$$

Additionally to the Hamiltonian, both the DNLS and the AL-NLS equation conserve a quantity that is commonly referred to as the norm or power of the solution

$$P_{DNLS} = \sum_{n=-\infty}^{\infty}|u_n|^2, \qquad (2.23)$$

while for the AL-NLS equation it is

$$P_{AL\text{-}NLS} = \sum_{n=-\infty}^{\infty}\frac{1}{\beta}\log\left(1 + \beta|u_n|^2\right). \qquad (2.24)$$

This conservation law, analogously to the corresponding conservation law for the continuum NLS equation, mirrors the U(1) symmetry or gauge invariance of the discrete model, i.e., its invariance with respect to an overall phase factor.

One of the fundamental differences between the DNLS and the AL-NLS model is the existence of a momentum conservation law in the latter which is *absent* in the former. In particular, the momentum

$$M = i\sum_{n=-\infty}^{\infty}\left(u_{n+1}^{\star}u_n - u_{n+1}u_n^{\star}\right) \qquad (2.25)$$

is conserved in the case of the AL-NLS model; this, in turn, implies that its localized solutions can be centered *anywhere* within the discrete lattice. In fact, in the AL-NLS case, there exist exact soliton solutions which are of the form (for simplicity, setting $\epsilon = -\beta/2 = 1$)

$$u_n = \sinh(\gamma)\mathrm{sech}\left(\gamma(n - \xi)\right)\exp\left(i\delta(n - \xi) + \rho\right), \qquad (2.26)$$

where $\dot{\xi} = 2\sinh(\gamma)\sin(\delta)/\gamma$ and $\dot{\rho} = -2 + 2\cos(\delta)\cosh(\gamma) + 2\delta\sin(\delta)\sinh(\gamma)/\gamma$ [8]. Then, the translational invariance is evident in the presence of an undetermined integration constant in the ordinary differential equation (ODE) for the time evolution of the position of the soliton center ξ.

In the DNLS case, the absence of translational invariance no longer permits to the solution to be arbitrarily centered anywhere along the lattice. Instead, there are only *two* stationary solutions (modulo the integer shift invariance of the lattice),
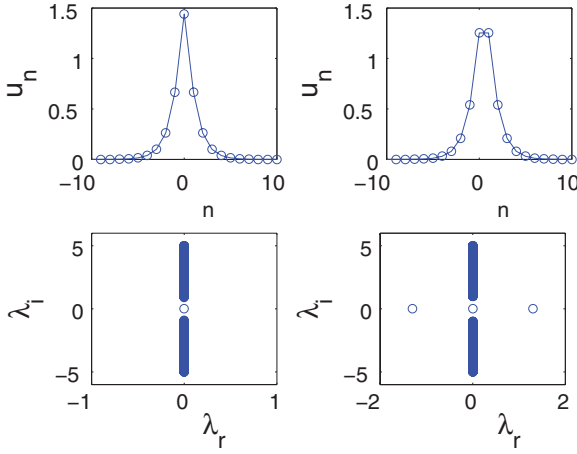
Fig. 2.2 The *top panel* shows the discrete on-site solitary wave (*left*) and inter-site solitary wave (*right*) for $\epsilon = 1$. The *bottom panels* show the corresponding linear stability eigenvalues, illustrating the linear stability of the former and linear instability of the latter (due to a real eigenvalue pair). There is only a single pair of eigenvalues at the origin, due to the phase invariance; note also the upper bound of the continuous spectrum (a feature absent in the continuum limit, where the continuous spectrum extends to $\pm i\infty$)

one centered on a lattice site (on-site) and one centered between two adjacent lattice sites (i.e., inter-site or bond-centered solution). These two solutions are shown in the top panels of Fig. 2.2. Such localized modes were initially proposed in a different dynamical lattice context in [9] and [10]; a relevant discussion of these modes in DNLS can be found in [11].

A fundamental level of understanding of this feature (although partially heuristic) can be obtained by using the continuum soliton solution of Eq. (2.10) as an *ansatz* in the formula for the *discrete energy* of Eq. (2.17). This is a "collective coordinate" type approach using as the relevant coordinate the position of the pulse center x_0. The resulting expression for the (discrete) Hamiltonian is given by

$$H_{DNLS} = \frac{16\pi^2}{h^2} \sum_{m=1}^{\infty} \frac{m \cos\left(\frac{2\pi m x_0}{h}\right)}{\sinh\left(\frac{m\pi^2}{\sqrt{\Lambda}h}\right)} \left[\epsilon - \frac{\Lambda}{3}\left(1 + \frac{m^2\pi^2}{\Lambda h^2}\right)\right], \qquad (2.27)$$

where it should be kept in mind that $\epsilon = 1/h^2$. To derive the above expression [12], terms independent of x_0 have been neglected in the energy (cf. also with the momentum invariant for the AL lattice and its relevant calculation in [13]), and the Poisson summation formula [14] has been critically used, according to which

$$\sum_{n=-\infty}^{\infty} f(\beta n) = \frac{\sqrt{2\pi}}{\beta} \sum_{m=-\infty}^{\infty} F\left(\frac{2m\pi}{\beta}\right), \qquad (2.28)$$

where F is the Fourier transform of f,

$$F(k) = \frac{1}{\sqrt{2\pi}} \int_{-\infty}^{\infty} f(x)e^{ikx}dx. \tag{2.29}$$

The above calculation yields the so-called Peierls–Nabarro (PN) [15, 16] potential which is famous from the theory of crystal dislocations representing the energy landscape that a dislocation faces in a crystal lattice. Of particular importance is the so-called PN barrier, namely the energy barrier that needs to be overcome in order for the coherent structure to travel a distance of one lattice site. In the present setting, the PN barrier can be easily found from the above expression for H_{DNLS} to be

$$H_{PN} = \frac{32\pi^2}{h^2} \sum_{m=1}^{\infty} \frac{m(1-(-1)^m)}{\sinh\left(\frac{m\pi^2}{\sqrt{\Lambda}h}\right)} \left[\epsilon - \frac{\Lambda}{3}\left(1 + \frac{m^2\pi^2}{\Lambda h^2}\right)\right]. \tag{2.30}$$

(We will not attempt to evaluate this expression and compare it with numerical results for reasons that will be explained in Part II).

However, the expression of Eq. (2.30) bears an additional piece of information. In the continuum limit of $h \to 0$, the above examined energy is *independent* of the position of the pulse center due to the translational invariance of the continuum model, i.e., $H(x_0)$ is a *constant* function of x_0. Therefore, in the case where the symmetry is broken (for $h \neq 0$), the height of the periodic energy barrier represents a quantitative measure of "how much" the invariance is broken. This amount appears, in Eq. (2.30), to be *exponentially small* in the relevant parameter which is the lattice spacing h (note the dominant hyperbolic sine terms in the denominator proportional to $\sinh(m\pi^2/\sqrt{\Lambda}h)$). It is perhaps interesting to attempt to justify this exponential smallness in a qualitative way as follows: if we try to expand the operator $\Delta_2 u_n$ by means of a Taylor expansion, we obtain

$$\Delta_2 u_n = \sum_{j=1}^{\infty} \frac{2h^{2j}}{(2j)!} \frac{d^{2j}u}{dx^{2j}}. \tag{2.31}$$

However, *to all algebraic orders* in this power-law expansion of the discrete operator, the right-hand side of Eq. (2.31) contains *derivatives*. However, derivatives are translationally invariant objects. Hence, in order to be able to observe the *breaking* of the symmetry, one has to go *beyond all algebraic orders* in the power-law expansion and hence has to become *exponentially small* in h, just as the energy landscape of Eq. (2.27) suggests.

We are now in a position to discuss the linear stability problem at the discrete level of the DNLS equation. Starting with the linear stability ansatz through the discrete analog of Eq. (2.11) (where each term should be thought of as having a subscript n indexing the lattice sites), we obtain the analog of the eigenvalue equations (2.12) and (2.13) for Eq. (2.1)

$$\lambda v_n = L_- w_n = (-\epsilon \Delta_2 + \Lambda - \beta u_{0,n}^2) w_n, \qquad (2.32)$$

$$\lambda w_n = -L_+ v_n = -(-\epsilon \Delta_2 + \Lambda - 3\beta u_{0,n}^2) v_n. \qquad (2.33)$$

In the lattice case, Eqs. (2.32) and (2.33) represent a matrix eigenvalue problem for the eigenvalues λ and the eigenvectors $(v_n, w_n)^T$ that is subsequently solved numerically.

A small remark should be added here about eigenvalue notation. In the physics literature, it is quite common to use the eigenfrequency ω, while in the more mathematically oriented texts, $\lambda = i\omega$ is used to denote eigenvalues. The two notations will be used interchangeably, with the understanding that linear instability is implied by non-zero imaginary part of ω or, equivalently, by the non-zero real part of λ.

The following features are generically observed in spectral plots analogous to the ones shown in Fig. 2.2 but for different values of the coupling strength ϵ:

- The continuous spectrum of plane wave eigenfunctions $\sim \exp(\pm i(qn - \omega t))$, exists also in the discrete problem and satisfies the following dispersion relations:

$$\omega = \Lambda + 4\epsilon \sin^2\left(\frac{q}{2}\right), \qquad (2.34)$$

$$\omega = -\Lambda - 4\epsilon \sin^2\left(\frac{q}{2}\right). \qquad (2.35)$$

  As seen from Eqs. (2.34) and (2.35), this branch of the spectrum extends over the interval $\pm[\Lambda, \Lambda + 4\epsilon]$ (along the imaginary axis of the spectral plane).
- In addition, as indicated above, the preservation of the U(1) invariance under discretization leads to a pair of eigenvalues $\lambda^2 = 0$.
- The translational invariance breaking is, as argued above, one of the key features of the discrete problem in comparison to its continuum sibling. In the case of a site-centered (linearly stable) solution, as shown in Fig. 2.2 and justified later in this chapter, the bifurcation of the translational eigenvalues occurs along the imaginary axis, leading to linear stability. On the contrary, in the case of the bond-centered solutions, the breaking of the symmetry leads to bifurcation along the real axis, rendering such inter-site-centered solutions linearly unstable.
- Finally, as was originally illustrated in [17] and subsequently expanded in [5], as the lattice spacing increases (and the coupling strength $\epsilon = 1/h^2$ decreases), there is also a pair of eigenmodes that bifurcates from the lower edge of the continuous spectrum, becoming a point spectrum eigenvalue. This, so-called, internal mode bifurcation does not affect critically the stability of the fundamental solution (at least, in the one-dimensional problem – in higher dimensions, as we will see below in Chap. 3, Sect. 3.3.4, such bifurcations may affect the stability critically), as will be quantified in what follows.

The above information yields the full spectral information in the case of a fundamental solution (single pulse) (we will see below how this picture is modified for multipulse waveforms). In what follows, we attempt to quantify some of the features

of the single-pulse linearization spectrum, namely the exponential bifurcation of the translational eigenvalue and the exponential, as well as power-law bifurcation of the internal mode from the band edge of the continuous spectrum.

We start by trying to capture the exponential bifurcation of the translational eigenmode using a more rigorous method. Specifically, we will use the discrete Evans function method developed in [18]. Here, we will outline the basic features of the method (we refer the reader to the original work of [18] for more details).

The eigenvalue problem can also be written as a first-order system

$$Y_{n+1} = A(\lambda, n)Y_n \tag{2.36}$$

with $\lambda = i\omega$. Equation (2.36) has solutions, Y^+ (Y^-) that decay exponentially as $n \to +\infty$ ($n \to -\infty$). Forming the wedge product of the two, we obtain an analytic function, the so-called Evans function, whose zeros, *by construction*, pertain to eigenvectors that span the subspace of intersection of the two spaces and hence decay for $n \to \pm\infty$. Hence, if we define

$$E(\lambda) = Y^+ \wedge Y^-, \tag{2.37}$$

the solutions of the linearization problem, λ, such that $E(\lambda) = 0$ form the *point spectrum* of eigenvalues with localized eigenfunctions in the linearization problem.

In order to evaluate the Evans function for the DNLS problem, we can use its analytic properties and Taylor expand it close to the origin of the spectral plane. To do this for the DNLS equation, we consider it as a perturbation of the AL-NLS equation. In the calculation below, for reasons of convenience, we will consider the case of $\epsilon h^2 = -\beta/2 = 1$ in Eq. (2.1); we will also denote the steady-state solution by v_n. Then, the steady-state problem can, upon setting $r_n = (v_n - v_{n-1})/h$, be rewritten as

$$v_{n+1} = \left(1 + \frac{h^2}{1 + h^2 v_n^2} \left(\Lambda - 2v_n^2\right)\right) v_n + hr_n + \varepsilon \frac{h^2 v_n^3}{1 + h^2 v_n^2} \left(\Lambda - 2v_n^2\right), \tag{2.38}$$

$$r_{n+1} = \frac{h}{1 + h^2 v_n^2} \left(\Lambda - 2v_n^2\right) v_n + r_n + \varepsilon \frac{hv_n^3}{1 + h^2 v_n^2} \left(\Lambda - 2v_n^2\right).$$

The above equation is written so that the limit of $\varepsilon = h^2 = 0$, Eq. (2.38), is the steady-state problem for the AL-NLS equation.

In the case of $\varepsilon = 0$, the exact (single soliton) solution of the AL-NLS equation is given by

$$Q_n(\xi) = \sqrt{\Lambda} \sinh(\alpha)\text{sech}(\tilde{\alpha}n + \xi), \tag{2.39}$$

where

$$\cosh(\tilde{\alpha}) = 1 + \frac{\Lambda h^2}{2} \quad \text{and} \quad \sinh(\alpha) = \frac{\sinh(\tilde{\alpha})}{\sqrt{\Lambda}\, h}.$$

In that case, it is also true that the steady-state problem has an infinite number of invariants $\cdots = I_n = I_{n+1} = \cdots = \text{const.}$ I_n is given by

$$I_n = h^2 v_n^2 v_{n-1}^2 + v_n^2 + v_{n-1}^2 - 2\mu v_n v_{n-1} \tag{2.40}$$

with $\mu = 1 + \Lambda h^2/2$.

Hence, following Ablowitz and Herbst [19, 20], in the perturbed (DNLS) case of $\varepsilon \neq 0$, the Melnikov function can be calculated as

$$\varepsilon M(\xi, \varepsilon) = \sum_{n=-\infty}^{\infty} \Delta_n I(\xi, \varepsilon) = \sum_{n=-\infty}^{\infty} \left[I(\mathbf{x}_{n+1}) - I(\mathbf{x}_n) \right], \tag{2.41}$$

where I is as defined above but in the $\varepsilon \neq 0$ case, it is no longer a constant. Equations (2.38) can be expressed in the form $\mathbf{x}_{n+1} = F(\mathbf{x}_n) + \varepsilon G(\mathbf{x}_n)$. Using this notation and Taylor expanding $H(F(\mathbf{x}_n) + \epsilon G(\mathbf{x}_n))$, we obtain for M the expression

$$M(\xi, \varepsilon) = \sum_{n=-\infty}^{\infty} \nabla I(\mathbf{x}_{n+1}) G(\mathbf{x}_n; \varepsilon). \tag{2.42}$$

This allows us to evaluate the Melnikov function (see [18] for details), up to corrections of $O(e^{-2\pi^2/\tilde{\alpha}})$, as

$$M(\xi, h) = C(h) e^{-\pi^2/\tilde{\alpha}} \sin\left(\frac{2\pi\xi}{\tilde{\alpha}} \right),$$

where

$$C(h) = 4\pi \frac{h}{\tilde{\alpha}} \left(\frac{2}{45} \frac{\pi^2}{\tilde{\alpha}^2} + \frac{2}{9} \frac{\pi^4}{\tilde{\alpha}^4} + \frac{8}{45} \frac{\pi^6}{\tilde{\alpha}^6} \right) \approx \frac{2147.8}{h^6}. \tag{2.43}$$

In the case of the AL-NLS equation, the "effective" (since ξ in Eq. (2.39) can take any value) translational invariance ensures that the stable and unstable manifolds of the homoclinic orbit intersect non-transversely. On the other hand, in the non-integrable case of the DNLS and generically (for $\varepsilon \neq 0$) this non-transversality will not persist. In fact, the splitting of the orbits (or effectively the angle of intersection of the manifolds) is given by the Melnikov function. Hence, in essence, the Melnikov function is a measure of the breaking of translational invariance and is expected to be transcendentally small (as in our previous calculation). This exponentially small splitting is associated with the above discussed PN barrier.

Having evaluated the Melnikov function, we can now proceed to the Taylor expansion of the Evans function of the DNLS equation, as a perturbation to the AL-NLS problem. In particular, the Evans function E is a function of the eigenvalue λ and the perturbation strength ε. Since for the AL-NLS equation $E(\lambda = 0; \epsilon = 0)$

$= 0$, we need to find the leading order derivatives with respect to ε and λ. As λ is an eigenvalue of algebraic multiplicity four in the AL lattice, the first derivative that will yield a non-zero contribution is $\partial_\lambda^4 E(0;0)$, which will generically be constant. The tools developed by Kapitula and co-workers [21–23] can then be used to obtain this constant. Furthermore, the preservation of the phase invariance and the bifurcation of merely the translational pair of eigenvalues in the DNLS case implies that the leading order derivative with respect to ε of non-zero contribution will be $\partial_\varepsilon \partial_\lambda^2 E(0;0)$. However, due to its relation with the splitting of the orbits of the perturbed problem, this derivative will generically be $\sim \partial_\xi M(\xi;\varepsilon)$, as can be shown on general grounds (see, e.g., [18]). The Taylor expansion of the Evans function will therefore read

$$E(\lambda;\varepsilon) = \varepsilon \lambda^2 \partial_\varepsilon \partial_\lambda^2 E(0;0) + \lambda^4 \partial_\lambda^4 E(0;0) \tag{2.44}$$

and the calculation of the details specific to the DNLS equation yields

$$E(\lambda;h^2) \sim \lambda^2 (h^2 \partial_\xi M(\xi;h^2) + 2B\lambda^2), \tag{2.45}$$

where B is a constant. Substituting the expression for the Melnikov function, we conclude that for the site-centered mode (that was numerically found to be stable previously)

$$\lambda_s^\pm \sim \pm i \sqrt{\frac{\pi h^2 C(h)}{B_1 \tilde{\alpha}}} \, e^{-\pi^2/2\tilde{\alpha}}, \tag{2.46}$$

while for the inter-site-centered mode (that was previously found numerically to be unstable due to a real eigenvalue pair)

$$\lambda_u^\pm \sim \pm \sqrt{\frac{\pi h^2 C(h)}{B_1 \tilde{\alpha}}} \, e^{-\pi^2/2\tilde{\alpha}}. \tag{2.47}$$

The results of Eqs. (2.46) and (2.47) confirm the validity of the numerical findings. Furthermore, the Evans function method naturally demonstrates how the exponentially small transversality effects of (translational invariance) symmetry breaking are mirrored in the bifurcation of the translational eigenmodes away from the origin of the spectral plane. The predictions of the Evans method are compared with the results of the linear stability analysis in Fig. 2.3.

Having analyzed the bifurcation of the translational mode (note that for the inter-site-centered solution, we will discuss a different limit later in this chapter), we now turn our attention to the other interesting feature caused by discreteness as a perturbation to the continuum problem. As was first observed for kinks in a modified sine-Gordon potential [24] and later elaborated for kinks in nonlinear Klein–Gordon lattices and for standing waves in DNLS lattices in [5, 17, 18, 25–27], localized
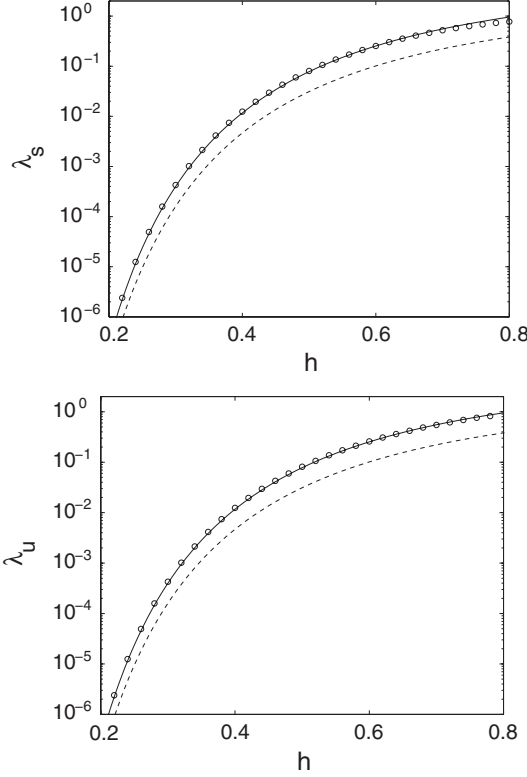
Fig. 2.3 The Evans function prediction for the imaginary eigenvalue of the site-centered mode (*top panel*) and for the real eigenvalue of the inter-site-centered mode (*bottom panel*). The theoretical results given by Eqs. (2.46) and (2.47), respectively, capture the functional dependence but not the exact prefactor. The result of Eqs. (2.46) and (2.47) without the corrected prefactor is shown by the dashed line. The result with the corrected prefactor is the solid line and it is in excellent agreement with the numerical results for the bifurcation of the corresponding translational eigenvalue given by the circles. The prefactors need to be corrected since, as explained in [18], the Evans function method captures the leading order functional dependence (on *h*) but higher order contributions to the prefactor are not accounted for by this method. Reprinted from [18] with permission

eigenmodes may bifurcate from the bottom edge of the continuous spectrum ($\omega_p = \pm\Lambda$ for the DNLS equation) and subsequently be present in the gap between the band edge and the origin of the spectral plane as a point spectrum eigenvalue.

This phenomenon was first tackled theoretically in the framework of intrinsic localized modes (ILMs) in [17]. In this work, discreteness was considered as a leading order power-law perturbation to the continuum problem, using the Taylor expansion of Eq. (2.31):

$$i\psi_t + \psi_{xx} + 2|\psi|^2 u + \frac{h^2}{12}\psi_{xxxx} = 0. \tag{2.48}$$

Considering the last term in Eq. (2.48) as a perturbation (of strength $\delta = h^2/12$) and using leading order perturbation theory, a corrected solution can be obtained for the perturbed problem $\psi = \exp(it)(v_0(x) + \delta v_1(x))$, with

$$v_1(x) = \frac{1}{2}\left(\frac{x\sinh(x)}{\cosh^2(x)} - \frac{7}{\cosh(x)} + \frac{8}{\cosh^3(x)}\right). \tag{2.49}$$

Then, the perturbed linearization problem of Eqs. (2.12) and (2.13) can be written as

$$U'' + \left(\frac{6}{\cosh^2 x} - 1\right)U + \omega W + (\partial_x^4 + 12v_0v_1)\delta U = 0, \tag{2.50}$$

$$W'' + \left(\frac{2}{\cosh^2 x} - 1\right)W + \omega U + (\partial_x^4 + 4v_0v_1)\delta W = 0. \tag{2.51}$$

Assuming now the eigenvalue bifurcating from the bottom of the continuous band edge to have a frequency $\omega = 1 - \delta^2\kappa^2$ (where $\delta = h^2/12$ is the measure of the perturbation), the authors of [17] project the new basis of continuous eigenfunctions $[U, W]^T$ onto the known old one [4]. Assuming that the eigenvalue bifurcating from the band edge is given by the above expression, the integral equation resulting from the projection, in the case of wave number $k = 0$ yields a solvability condition that allows to determine κ as (in the case of the DNLS equation)

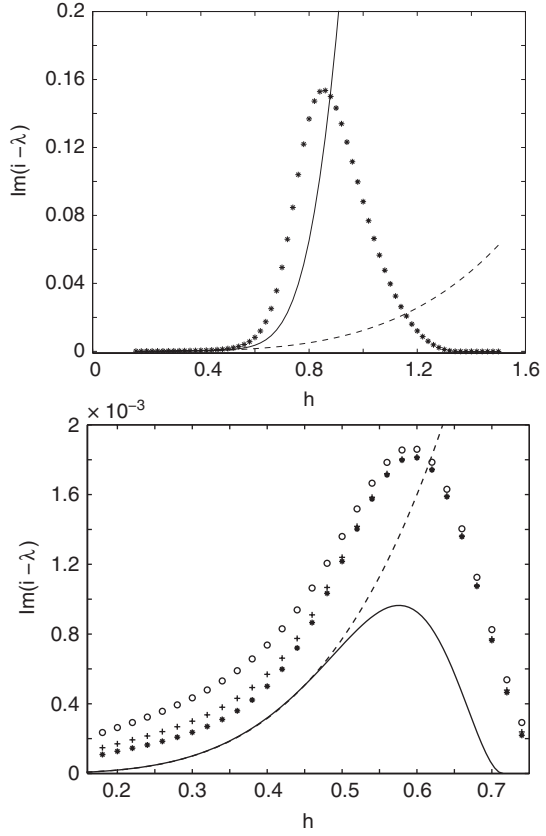$$|\kappa| = \frac{\text{sgn}(\delta)}{4}\int U(x,0)f_1(x)U(x,0) + W(x,0)f_2(x)W(x,0)dx, \tag{2.52}$$

where $f_{1,2}$ correspond to the perturbative operator prefactors of δU and δW in Eqs. (2.50) and (2.51), respectively. This method yields $\kappa = 4/3$ in the case of DNLS and hence

$$\omega = 1 - \frac{h^4}{81}. \tag{2.53}$$

However, as can be seen from the above methodology, only the leading order power-law correction is recovered in this way. One of the major disadvantages of this result is that it does *not* distinguish between the bifurcation of the eigenvalue pair (the "breathing" mode according to [5]), of the stable site-centered and the unstable inter-site-centered wave. Such differences, obvious in Fig. 2.4, can only be attributed to exponentially small differences between the two waves.

For this reason, in [18, 27], the Evans function methodology was developed in the vicinity of the branch point $\omega = 1$ ($\lambda = i$). However, in this case both exponential *and* power-law terms were present in the derivative of E with respect to the O(ε) perturbation in Eqs. (2.38). Evaluation of the relevant partial derivatives and Taylor expansion of $E(\lambda; \epsilon)$ near $\lambda = i; \epsilon = 0$, performed in detail in [18], yields

Fig. 2.4 Bifurcation of the eigenvalue λ of the breathing mode of the stable and unstable wave from the edge of the continuous spectrum ($\lambda = i$) as a function of the lattice spacing h; the dashed line shows the theory of [17], the solid line the theory of [18, 27], and the stars the results of numerical experiments on a 400-site lattice with periodic boundary conditions. In the bottom panel, circles indicate results on 200-site and plus symbols on a 300-site lattice. Reprinted from [18] with permission

$$E(\gamma, h) = 4h^{-1}\left[\gamma - \frac{h^3}{9}\left\{1 + \frac{9}{4}C(h)e^{-\pi^2/\tilde{\alpha}}\cos\left(\frac{2\pi\xi}{\tilde{\alpha}}\right)\right\}\right], \qquad (2.54)$$

where

$$\gamma^2 = (1 + i\lambda)h^2\left(1 + \frac{1}{4d^2}\right). \qquad (2.55)$$

Setting $E = 0$, we obtain an expression for the eigenvalue bifurcation

$$\lambda(\xi) = i\left[1 - \frac{h^4}{81}\left\{1 + \frac{9}{2}C(h)e^{-\pi^2/\tilde{\alpha}}\cos\left(\frac{2\pi\xi}{\tilde{\alpha}}\right)\right\}\right]. \qquad (2.56)$$

Since ξ can take the values $n\tilde{\alpha}$ or $(n + 1/2)\tilde{\alpha}$, we obtain different eigenvalue bifurcations for the site-centered and the inter-site-centered modes. $C(h) =$

$(256\pi)/(45)(\pi/\tilde{\alpha})^7 \approx 53979.2\,h^{-7}$. It should be noted, however, that to leading (power law) order this result is the same as the one of [17]. On the other hand, as can be observed in the numerical results of Fig. 2.4, there is a significant difference between the bifurcation of the stable and the unstable wave. In fact, the numerical experiment shows that the maximal bifurcation for the former is ≈ 0.155, while for the latter it is only ≈ 0.0019. Hence, the difference between the two waves, which is discernible only at an exponentially small level of description, turns out to be important. Equation (2.56) renders this distinction clear, as it suggests that for $h > 0.45$ the exponential effects become important. This distinction has also been observed in nonlinear Klein–Gordon lattices. For instance, in the discrete sine-Gordon model, the bifurcation of the edge or breathing mode of the unstable wave is completely *suppressed* by the exponential contributions, while the bifurcation does take place for the stable wave [25].

So far, we have clarified the questions pertaining to linear stability of the site-centered and inter-site-centered modes. However, it is also important to know whether information about linear stability can be generalized to nonlinear stability of the relevant waves. This is often not possible, however, in the case of the fundamental solutions and in the vicinity of the continuum limit $h \to 0$, the work of [28] can be used to obtain nonlinear stability conclusions. Suppose that the operator L_+, defined in Eq. (2.13) has only one eigenvalue $\lambda \leq 0$, and suppose that the only eigenvalue of L_-, given in Eq. (2.12), that has the property $\lambda \leq 0$ is exactly at $\lambda = 0$. Furthermore, suppose that

$$\frac{d}{d\omega}P > 0. \tag{2.57}$$

Then it can be shown using the work of [28] that the wave is nonlinearly stable. As $h \to 0^+$ the wave is approximately given by $\sqrt{\omega}\,\mathrm{sech}(\sqrt{\omega}\,x)$. Hence,

$$\lim_{h \to 0^+} P = \int_{-\infty}^{+\infty} \left(\sqrt{\omega}\,\mathrm{sech}(\sqrt{\omega}\,x)\right)^2 dx = 2\sqrt{\omega}$$

so that

$$\lim_{h \to 0^+} \frac{d}{d\omega}P > 0.$$

Hence, the condition of Eq. (2.57), is satisfied for small h.

It is clear that $L_-(v_n) = 0$ so that $\lambda = 0$ is an eigenvalue of L_-. Since v_n is a positive solution, Sturm–Louiville theory states that $\lambda = 0$ is the minimal eigenvalue. At small h, the operator L_+ is a perturbation of the corresponding operator for the AL-NLS equation. For the AL-NLS equation the operator is such that $\partial_\xi v_n$ is an eigenfunction at $\lambda = 0$. Thus, by another application of Sturm–Liouville theory, one has that there exists one negative eigenvalue which is of O(1). Upon perturbation, both of the eigenvalues will move by an exponentially small amount. Hence, it is enough to track the eigenvalue near zero in order to determine whether the first

condition above is met. However, according to the theory of [28, 29], the wave is linearly unstable if the operator L_+ has two strictly negative eigenvalues. One can conclude (by contradiction) that for the linearly unstable wave (inter-site-centered solution) the zero eigenvalue of the AL-NLS equation must move to the left in the case of the DNLS equation, while for the linearly stable wave (site-centered solution) the zero eigenvalue of the AL-NLS equation must move to the right. Thus, we have shown that if $h > 0$ is sufficiently small, for the linearly stable on-site wave, the first condition is also met and consequently the wave is also *nonlinearly stable*.

2.1.2 The Anti-Continuum Approach

We now approach the same problem, namely the existence and stability of single pulses in the DNLS equation from an entirely different perspective, that was originally proposed by MacKay and Aubry [30] and has been extensively used in the literature since. This is the initially referred to as anti-integrable, and later more appropriately termed the anti-continuum (AC) limit of $\epsilon = 0$. In this limit, the sites are *uncoupled* and it is straightforward to solve the ensuing ordinary differential equations for u_n. The key question then becomes which ones of the possible combinations of the different u_n's will persist, as soon as the coupling between the sites is turned on (i.e., $\epsilon \neq 0$). To present the relevant analysis, let us use Eq. (2.1) with $\beta = -1$ (i.e., in the focusing case) and having made a transformation of the field $u_n \to u_n \exp(-2i\epsilon t)$, as is always possible due to the gauge invariance. Then (2.1) acquires the form

$$i\dot{u}_n = -\epsilon(u_{n+1} + u_{n-1}) - |u_n|^2 u_n. \tag{2.58}$$

As before, we look for standing waves of the form: $u_n = \exp(i\mu t)v_n$ which, in turn, satisfy the steady-state equation

$$\left(\mu - |v_n|^2\right) v_n = \epsilon \left(v_{n+1} + v_{n-1}\right). \tag{2.59}$$

In the AC limit, it is easy to see that Eq. (2.59) is completely solvable $v_n = 0, \pm\sqrt{\mu}\exp(i\theta_n)$, where θ_n is a *free* phase parameter for *each* site. However, as indicated above, out of this huge freedom of phase selection for each site in the uncoupled limit, the important consideration is how much of it remains as soon as the cross-talking between sites is allowed. A simple way to address this question in an explicit way in the one-dimensional case of Eq. (2.58) is to multiply Eq. (2.59) by $v_n^\star$ and subtract the complex conjugate of the resulting equation, which in turn leads to

$$v_n^\star v_{n+1} - v_n v_{n+1}^\star = \text{const} \Rightarrow 2\arg(v_{n+1}) = 2\arg(v_n), \tag{2.60}$$

where we have used the fact that the constant should be equal to 0 since we are considering solutions vanishing as $n \to \pm\infty$. The scaling freedom of the equation allows us to select $\mu = 1$ without loss of generality. Then, this yields the important conclusion that the *only* states that will persist for finite ϵ are ones containing sequences with combinations of $v_n = \pm 1$ and 0. A systematic computational classification of the simplest ones among these sequences and of their bifurcations is provided in [31]. It should be mentioned also in passing that although we considered here the focusing case of $\beta = -1$, the defocusing case of $\beta = 1$ can also be addressed based on the same considerations and using the so-called staggering transformation $w_n = (-1)^n u_n$ (which converts the defocusing nonlinearity into a focusing one).

Although we will use the above considerations later in this chapter, when considering the case of multipulses, in the present subsection, we focus on the single-pulse case. It turns out that the single pulse exists in the DNLS "all the way" between the continuum and the AC limit (a very rare feature, as can be inferred, e.g., from Fig. 14 of [31]). In fact, there are *two* waveforms at the AC limit that will both result to the continuum pulse as $\epsilon \to \infty$ ($h \to 0$). One of them is the configuration with $v_n = \delta_{n,n_0}$, i.e., the single-site excitation. The other is the configuration with $v_n = \delta_{n,n_0} + \delta_{n,n_0+1}$, i.e., a two-site, bond-centered, in-phase excitation. Since the latter is a multisite structure, it will be examined in more detail later in this chapter (where the general theory of multisite excitations will be developed). Incidentally, these two are the *only* configurations that persist throughout the continuation from the AC to the continuum limit.

We also briefly discuss the stability near the AC limit. Once again, the L_+ and L_- operators emerge when linearizing around the standing wave solutions of Eqs. (2.58) and (2.59) in the linearization problem of the form

$$\left(1 - 3v_n^2\right) a_n - \epsilon \left(a_{n+1} + a_{n-1}\right) = L_+ a_n = -\lambda b_n, \tag{2.61}$$

$$\left(1 - v_n^2\right) b_n - \epsilon \left(b_{n+1} + b_{n-1}\right) = L_- b_n = \lambda a_n. \tag{2.62}$$

It is perhaps relevant to note here that the eigenvalue problem has the general symplectic form $JLw = \lambda w$ where the J matrix has the standard symplectic structure ($J^2 = -I$), i.e.,

$$\mathcal{J} = \begin{pmatrix} 0 & I \\ -I & 0 \end{pmatrix} \tag{2.63}$$

and the operator L is defined as

$$L = \begin{pmatrix} L_+ & 0 \\ 0 & L_- \end{pmatrix}. \tag{2.64}$$

In the case of the AC limit of $\epsilon = 0$, the operators L_- and L_+ simplify enormously, becoming simply multiplicative operators. It is then straightforward to solve the ensuing eigenvalue problem for each site of the AC limit. Assume a sequence for v_n with N "excited" (i.e., $\neq 0$) sites; then, it is easy to see that for $\epsilon = 0$ these sites correspond to eigenvalues $\lambda_{L_+} = -2$ for L_+ and to eigenvalues $\lambda_{L_-} = 0$ for L_-, and they result in N eigenvalue pairs with $\lambda^2 = 0$ for the full Hamiltonian problem. On the other hand, all the remaining, infinitely many (non-excited) sites in the chain with $v_n = 0$ satisfy $a_n = -\lambda b_n$ and $b_n = \lambda a_n$. This yields a pair of eigenvalues $\lambda^2 = -1$, i.e., $\lambda = \pm i$ (more generally for a frequency Λ of the solution, these will be $\lambda = \pm i\Lambda$), with infinite multiplicity.

In the case we are currently considering, namely that of a single-site excitation that will eventually give rise to the single pulse of the continuum limit, there is only a single pair of zero eigenvalues, corresponding to the excited site. There are also infinitely many pairs, corresponding to the non-excited sites, at $\lambda = \pm i$ (or $\pm i\Lambda$ more generally). As soon as ϵ becomes non-zero, the former zero eigenvalue pair will have to *remain* at 0, because of the gauge (i.e., U(1)) invariance of the equation. On the other hand, the infinitely many sites with identical eigenvalues will "expand" in accordance with Eqs. (2.34) and (2.35). As ϵ is increased, the two eigenvalues of the top panels of Figs. 2.3 and 2.4 will bifurcate from the bottom edge of the continuous spectrum. One of these eigenvalues will approach the origin exponentially as $h \to 0$, while the other, upon a maximal excursion from the continuous spectrum's lower band edge, it will return to it as $h \to 0$. This is the full spectral picture joining the results of the continuum to those of the AC limit. While we have described analytically both the $h \to 0$ limit in the previous subsection, and the $h \to \infty$ limit in this subsection, the intermediate region can only be quantified numerically, as is done in Figs. 2.3 and 2.4, as well as in Fig. 2.5 in a more conclusive way, giving information about all the point spectrum eigenvalues of the DNLS problem, as a function of the lattice spacing h.

Fig. 2.5 The figure shows the (non-zero) point spectrum eigenvalues as a function of the spacing h, as they are numerically obtained (in a 400-site computation) for the linearization around a single pulse of the DNLS equation. The solid line shows the internal mode that bifurcates from the bottom edge of the continuous spectrum and returns to it, while the dashed line shows the translational mode that exponentially approaches $\lambda^2 = 0$ as $h \to 0$
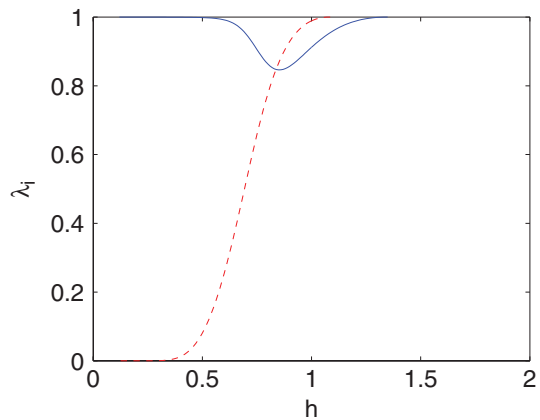
2.1.3 The Variational Approach

Another approach that yields quantitative semi-analytical information about the single-pulse case *even in the intermediate regime* is the so-called variational approach (VA). In the case of the DNLS, this was originally developed in [32] and was systematically tested recently in [33]. The VA (a detailed review of which can be found in [34]) consists of selecting an a priori ansatz for the form of the solution (in the case of the DNLS a typical, quantitatively tractable choice is $u_n = A \exp(-a|n|)$). It should be understood that this is a *dramatic* oversimplification of the solution. It reduces the original *infinite dimensional* dynamical system into a two-dimensional one, in the space of "adjustable parameters" A and a (representing measures of the amplitude and the inverse width of the pulse solution, respectively). This type of *ansatz* is not substituted in the steady-state (or dynamical) equation, which it cannot, by default, satisfy, since it is typically impossible to satisfy infinitely many equations with just two free parameters, unless, fortuitously, our ansatz represents an exact solution. It is, instead, substituted in the Lagrangian (either time-dependent, or when looking for steady states, time-independent). Subsequent derivation of the Euler–Lagrange equations (i.e., extremization of the action on the restricted subspace of the adjustable parameters) is performed in the expectation of obtaining a good fit to the corresponding infinite-dimensional extremization problem. This is a reasonable expectation provided that the waveform remains close to the ansatz, but may fail considerably when that is not the case. More importantly, it is not a priori obvious *when* the method will fail, although recent efforts are starting to aim toward systematically computing the relevant error and accordingly improving the approximation, when needed [35].

As an example, we now give the steady-state version of the variational approximation for a generalized DNLS problem in line with the original presentation of [32]. Consider the steady-state problem for the discrete waveform v_n

$$\Lambda v_n = \epsilon \left(v_{n+1} + v_{n-1} - 2v_n \right) + v_n^{2\sigma+1}, \tag{2.65}$$

which is the standing wave problem for a general power nonlinearity (as discussed in the beginning of this chapter). The case of $\sigma = 1$ corresponds to our familiar cubic DNLS. Equation (2.65) can be derived from the Lagrangian

$$L = \sum_{n=-\infty}^{+\infty} \left[\epsilon(v_{n+1} + v_{n-1})v_n - (\Lambda + 2\epsilon)v_n^2 + \frac{1}{\sigma+1} v_n^{2(\sigma+1)} \right]. \tag{2.66}$$

Substituting the above-mentioned simple exponential ansatz in the Lagrangian, one can perform the summation explicitly, which yields the *effective Lagrangian*,

$$L_{\text{eff}} = 2\epsilon P \operatorname{sech} a - (\Lambda + 2\epsilon)P + \frac{P^{\sigma+1}}{\sigma+1} \frac{\coth((\sigma+1)a)}{\coth^{\sigma+1} a}. \tag{2.67}$$

The (squared l^2) norm of the ansatz, which appears in Eq. (2.67), is given by

$$P \equiv \sum_{n=-\infty}^{+\infty} v_n^2 = A^2 \coth a. \tag{2.68}$$

The Lagrangian (2.67) gives rise to the variational equations, $\partial L_{\mathrm{eff}}/\partial P = \partial L_{\mathrm{eff}}/\partial a = 0$, which constitute the basis of the VA toward the computation of stationary waveforms [34]. They predict relations between the norm, frequency, and width of the fundamental pulses within the framework of the VA, namely

$$P^\sigma = \frac{4\epsilon \cosh^\sigma a \sinh^2(\sigma + 1)a}{\sinh^{\sigma-1} a(\sinh 2(\sigma + 1)a - \sinh 2a)}, \tag{2.69}$$

$$\Lambda = 2\epsilon(\operatorname{sech} a - 1) + P^\sigma \frac{\coth(\sigma + 1)a}{\coth^{\sigma+1} a}. \tag{2.70}$$

These ensuing transcendental equations connect the power of the pulse solution to its width (these are the two unknowns in these algebraic equations) and express these features as a function of the system parameters (such as the frequency Λ, the coupling strength ϵ, or the nonlinearity exponent σ). The equations can be solved with a standard computational mathematics package (i.e., such as the `FindRoot` routine in Mathematica) and compared to direct numerical computations, as is done in Fig. 2.6 (for $\Lambda = \sigma = 1$).

Figure 2.6 shows the continuum analog of the power of the pulse as a function of the lattice spacing h (the continuum limit of this quantity for the model considered herein can be easily seen to be 4, which is also confirmed by the relevant computations). It also shows the amplitude A of the discrete pulse as a function of the lattice spacing (the continuum limit for this quantity is $\sqrt{2}$), as well as the inverse width a as a function of h. One can easily note that for $h > 0.8$, the agreement between the variational solution of the greatly simplified 2×2 system of Eqs. (2.69) and (2.70) is truly *remarkable*. On the other hand, however, one has no a priori way to explain why the agreement starts becoming considerably worse for $h < 0.8$, other than to say that the oversimplified ansatz does not accurately describe the continuum, hyperbolic secant limit. However, a further quantification of the relevant statement cannot be a priori made. A deeper understanding of this discrepancy can, however, be partially obtained by considering the $a \to 0$ limit of the above equations (scaling out ϵ from Λ and P^σ), since we can see that $P^\sigma \approx (4 + 2\sigma + 2/\sigma)a^{2-\sigma}$, while $\Lambda \approx (1 + 2/\sigma)a^2$, as $a \to 0$. From these equations and Eq. (2.68), one can infer the dependence of the amplitude A on a as $A \approx (4 + 2\sigma + 2/\sigma)^{1/(2\sigma)}a^{1/\sigma}$. In the case of $\sigma = 1$, this yields $A \approx \sqrt{8}a \approx (2/\sqrt{3})\sqrt{2\Lambda} = (2/\sqrt{3})A_{cont}$, where A_{cont} denotes the amplitude of the continuum soliton. This indicates that in that limit the VA fails in capturing the amplitude by a factor of $2/\sqrt{3} \approx 1.15$. Nevertheless, the VA is often a useful tool in acquiring some insight on the nature of the full solution

Fig. 2.6 Results of the variational approximation: the *top panel* shows the analog of the continuum squared L^2 norm as a function of the lattice spacing h. The *solid line* represents the full numerical result, while the *dashed line* shows the result of the VA. The *bottom panel* curves have the same symbolism for the amplitude A of the solution (for which the fully numerical and variational results are again compared) and for the inverse width a of the pulse (for which only the variational result is given). It is worthwhile to note how efficient the VA is in capturing the full numerical result for $h > 0.8$
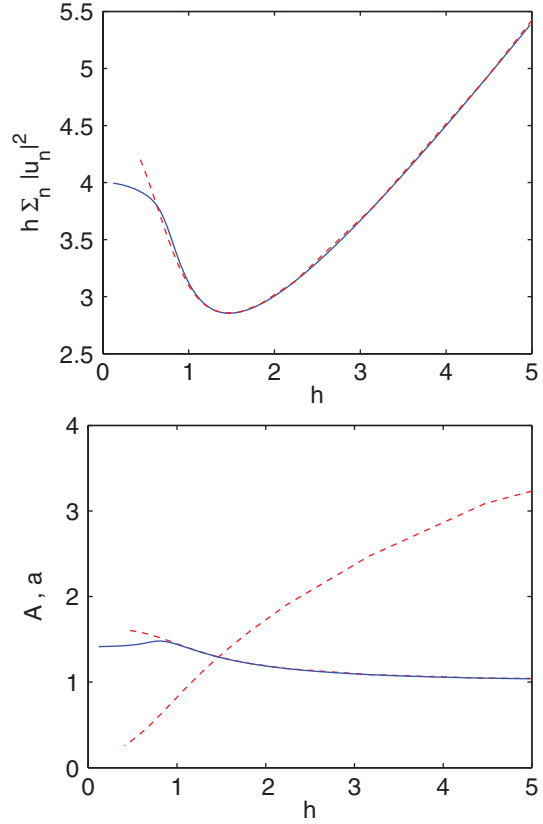
of the system and an understanding of its fundamental properties. Our argument here is that it should be used with the appropriate caution; furthermore, it has been our experience that it is a method that is considerably more likely to work with fundamental solutions (given a reasonable ansatz) than with higher order excited state solutions, whose (existence and stability) properties it is often unable to track.

Before closing this discussion about single-pulse solitary waves in this generalized DNLS model, it is interesting to refer to a particular effect that this model possesses for values of σ ranging between a lower and an upper critical one, namely *bistability* [32]. In particular, within this range of values of σ, for a given ϵ, the dependence of the l^2 norm as a function of Λ is not monotonic as it would be for $\sigma = 1$, but possesses a range of powers for which two stable solutions (with $dP/d\Lambda > 0$ and an unstable solution (with $dP/d\Lambda < 0$) coexist; see Fig. 2.7. The variational prediction captures this feature of the single-pulse state fairly accurately as is shown in the figure. Equivalently, this phenomenon also arises for fixed Λ as a function of the coupling ϵ. As a measure of the accuracy of the variational prediction, we give in Fig. 2.8 the full numerical result and how it compares with the semi-analytical prediction for the lower and upper critical σ for which bistability

Fig. 2.7 The (squared l^2) norm of the fundamental soliton family versus Λ for $\sigma = 1.5$. *Solid lines* display numerical results, while the *dashed curves* correspond to the predictions of the variational approximation
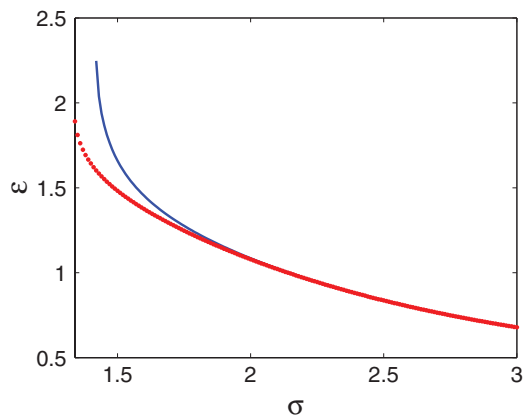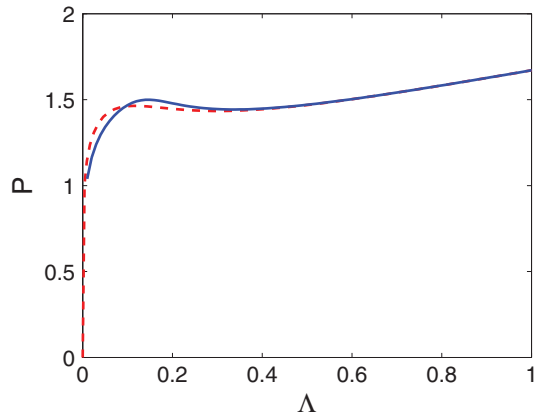
Fig. 2.8 Locations of the two bifurcations that account for the exponential destabilization and subsequent restabilization (the *top and bottom panels*, respectively) of the fundamental solitons (subject to the normalization $\Lambda \equiv 1$) in the plane of (σ, ϵ). The *line and dots* represent predictions of the variational approximation and numerical results, respectively. The restabilization corresponding to the bottom panel does not occur for $\sigma \geq 2$
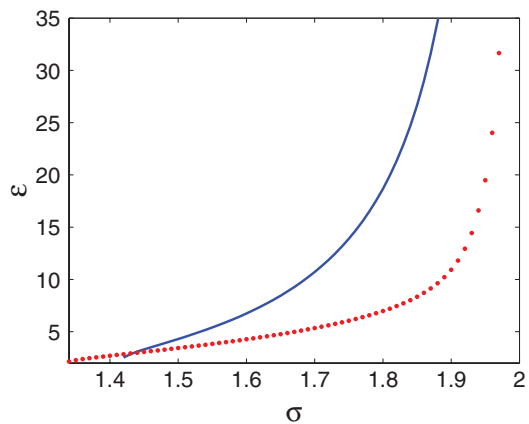
occurs as concerns their dependence on the coupling ϵ (or equivalently for a fixed σ, the lower and upper couplings between which the solution is unstable). It can be seen that the variational analysis captures the general trends of the relevant behavior but the partial inaccuracy of the relevant ansatz may not allow a good quantitative comparison between the two. We should also add in passing that beyond $\sigma = 2$, for dimension $d = 1$, equivalently to the case of $\sigma = 1$ for dimension $d = 2$, the continuum version of the model is subject to catastrophic collapse-type instabilities. This issue will be discussed, along with the discrete analog of such instabilities, in more detail in the two-dimensional (cubic) setting in Chap. 3.

2.2 Multipulse Solitary Waves

2.2.1 Multipulses Near the Anti-Continuum Limit

We now turn to the consideration of multipulse solitary waves, which we are going to examine chiefly starting from the AC limit of $\epsilon = 0$. In particular, in the latter case, instead of exciting a single site (which will result, as we saw above, in a single pulse), we excite N sites in the general case. In that case, considerations similar to the ones we presented above for the case of $\epsilon \neq 0$ indicate that in the one-dimensional setting, without loss of generality, we may concern ourselves only with excitations of each site which are either $u_n = 1$ or -1 (for frequency $\mu = 1$) while the rest of the (non-excited) sites have $u_n = 0$. Then, it is straightforward to see from the structure of the L_+ and L_- operators that for $\epsilon = 0$ the N excited sites correspond to eigenvalues $\lambda_{L_+} = -2$ for L_+ and to eigenvalues $\lambda_{L_-} = 0$ for L_-, and they result in N eigenvalue pairs with $\lambda^2 = 0$ for the full Hamiltonian problem. Hence, these eigenvalues are potential sources of instability, since for $\epsilon \neq 0$, $N-1$ of those will become non-zero (there is only one symmetry, namely the U(1) invariance, persisting for $\epsilon \neq 0$, retaining one pair of eigenvalues at the origin). The key question for stability purposes is to identify the location of these $N - 1$ small eigenvalue pairs.

To address the location of these eigenvalues in the presence of the perturbation induced by the inter-site coupling, one can manipulate Eqs. (2.61) and (2.62) into the form

$$\mathcal{L}_- b_n = -\lambda^2 \mathcal{L}_+^{-1} b_n \Rightarrow \lambda^2 = -\frac{(b_n, \mathcal{L}_- b_n)}{(b_n, \mathcal{L}_+^{-1} b_n)}. \tag{2.71}$$

Near the AC limit, the effect of L_+ is a multiplicative one (by -2). Hence,

$$\lim_{\epsilon \to 0} (b_n, \mathcal{L}_+^{-1} b_n) = -\frac{1}{2} \Rightarrow \lambda^2 = 2\gamma = 2(b_n, \mathcal{L}_- b_n). \tag{2.72}$$

   Therefore the problem translates into the determination of the spectrum of L_-.[1] However, using the fact that the standing wave solution v_n is an eigenfunction of L_- with $\lambda_{L_-} = 0$ and the Sturm comparison theorem for difference operators [36], one infers that if the number of sign changes in the solution at the AC limit is m (i.e., the number of times that adjacent to a $+1$ is a -1 or next to a -1 is a $+1$), then the number of negative eigenvalues $n(L_-) = m$ and therefore from Eq. (2.72), the number of imaginary eigenvalue pairs of $\mathcal{L}$ is m, while that of real eigenvalue pairs is consequently $(N-1) - m$. An immediate conclusion is that unless $m = N - 1$, or practically unless adjacent sites are out-of-phase with each other, the solution will be immediately unstable for $\epsilon \neq 0$. This eigenvalue count was presented in [37] although its stability consequences had been observed in numerous earlier works (see, e.g., [38] and references therein). It is also interesting to point out that a related count was originally presented in [39], although purely as an instability condition (rather than as a definitive count). In particular, it was recognized in that work that $n(L_-) = m$ and that that in the vicinity of the continuum limit (rather than the AC limit as here) each of the N pulses would have at least one negative eigenvalue associated with them, hence $n(L_+) \geq N$. Then, an important criterion was used that was originally developed in the work of Jones [29], namely that when $|n(L_+) - n(L_-)| > 1$, then a real eigenvalue pair will exist in the linearization. Hence, in the present case if $m < N - 1$, this criterion could be used to yield an instability, in agreement with the result presented above (but established in the vicinity of the AC limit).

   An important additional realization both in the work of [37] and in that of [39] was that the m negative eigenvalues of L_-, corresponding to the m imaginary pairs of the full linearization operator JL, have negative Krein signature. The Krein signature is a fundamental topological concept in the context of nonlinear Schrödinger equations (and Hamiltonian systems more generally); the interested reader should examine [40–45] for details and examples. These eigenvalues are often also mentioned in the physical literature as negative energy modes, see, e.g., [46–48]. For our present considerations, it suffices to say that this signature is essentially the signature of the energy surface and can be found to be equivalent to the sign of (w, L_-w). Hence, all of the m eigenvalue pairs bifurcating along the imaginary axis in our present calculation will be negative Krein signature (or negative energy) eigenvalues. The eigenvalues of negative Krein sign are well known to be *structurally unstable*. This means that small perturbations of the vector field can eject them off of the imaginary axis, leading to an unstable eigenvalue with a positive real part. Moreover, if eigenvalues of opposite sign collide, then they will generically form a complex conjugate pair after the collision, whereas if eigenvalues of the same sign collide, then they will pass through each other.

---

[1] It should be pointed out here that although Eq. (2.72) is particular to the cubic model, Eq. (2.71) is not and can straightforwardly be applied to any nonlinearity that depends on the field and its complex conjugate. The denominator of its right-hand side will in such cases typically provide a constant prefactor, while the spectrum of L_-, through considerations similar to those presented here, will determine the fate of small eigenvalues.

It is important to conclude from the above considerations that the only standing wave configuration of the discrete problem (starting from the AC limit) that will be structurally and nonlinearly stable is the single-site excitation. Not only did we establish nonlinear stability for that configuration above (near the continuum limit), but furthermore it is the only configuration (near the AC limit) that has neither a real eigenvalue pair (in which case it would be directly unstable) or an imaginary pair with negative Krein sign since $m = 0 = N - 1$. An additional remark worth making here concerns the case of the second solution of the AC limit reported in the previous section to eventually asymptote to the single-pulse configuration, namely the two-site, in phase excitation. In that case, $m = 0$, while $N = 2$, hence one can immediately see that for this waveform there will be $N - 1 - m = 1$ real eigenvalue pair, as soon as $\epsilon \neq 0$, indicating the instability of the relevant wave.

So far, we have used the above Eq. (2.72) in a qualitative way to obtain the relevant eigenvalue counts. In what follows, we also show how to use this equation in a quantitative manner, in order to obtain the dependence of the relevant eigenvalues on the model parameters (and, hence, wherever relevant, quantify the growth rate of the instability). To do so, we need to obtain a handle on the eigenvalues of the operator L_-. Considering the relevant eigenvalue problem $L_-\phi = \gamma\phi$, we can expand it in the vicinity of the AC limit, according to

$$L_- = L_-^{(0)} + \epsilon L_-^{(1)} + O(\epsilon^2), \tag{2.73}$$

$$\phi_n = \phi_n^{(0)} + \epsilon\phi_n^{(1)} + O(\epsilon^2), \tag{2.74}$$

$$\gamma = \epsilon\gamma_1 + O(\epsilon^2). \tag{2.75}$$

In this expansion,

$$L_-^{(0)}\phi_n = (1 - (v_n^{(0)})^2)\phi_n, \tag{2.76}$$

$$L_-^{(1)}\phi_n = -(\phi_{n+1} + \phi_{n-1}) - 2v_n^{(0)}v_n^{(1)}\phi_n, \tag{2.77}$$

where $v_n^{(0)}$ and $v_n^{(1)}$ correspond to the expansion $v_n = v_n^{(0)} + \epsilon v_n^{(1)}$ of the solution in the vicinity of the AC limit. The leading order correction $v_n^{(1)}$ will need to be computed from Eq. (2.59). It is straightforward to apply the expansion of the solution to the relevant equation (keeping in mind that $\mu = 1$ and the phases θ_n of the excited sites are $0, \pi$, corresponding to ± 1 field values). If we have the N excited sites adjacent to each other, then it is straightforward to find the leading order correction as

$$v_n^{(1)} = -\frac{1}{2}\left(\cos(\theta_{n-1} - \theta_n) + \cos(\theta_{n+1} - \theta_n)\right)e^{i\theta_n}, \quad 2 \leq n \leq N - 1, \tag{2.78}$$

$$v_1^{(1)} = -\frac{1}{2}\cos(\theta_2 - \theta_1)e^{i\theta_1}, \quad v_N^{(1)} = -\frac{1}{2}\cos(\theta_N - \theta_{N-1})e^{i\theta_N}, \tag{2.79}$$

$$v_0^{(1)} = e^{i\theta_1}, \quad v_{N+1}^{(1)} = e^{i\theta_N}, \tag{2.80}$$

while all other elements of $v_n^{(1)}$ are zero. Similarly, one can find the leading order corrections if the N adjacent sites are next nearest neighbor to each other (in that case, the leading order correction to the excited sites will be $v_n^{(2)}$), or for more distant initially excited sites (see [37] for such a calculation in the next-nearest-neighbor case).

If we have N excited sites at the AC limit, the relevant zero eigenvalue of the L_- operator as indicated above will have a multiplicity of N at the AC limit of $\epsilon = 0$. The corresponding linearly independent eigenvectors f_n can be conveniently selected to be $(0, \ldots, \pm 1, \ldots, 0)$ where the $\ldots$ indicate zeros and the ± 1 is located at the kth excited site for the kth eigenvector. Then the zero-order eigenvector $\phi^{(0)}$ can be expressed as a linear combination of the f_n's according to $\phi^{(0)} = \sum_{k=1}^{N} c_k f_k$, for appropriate choice of the coefficients c_k.

Our aim in this exercise is to perturbatively compute γ_1, the leading order correction to the zero eigenvalue of L_-, so that through the appropriate substitution to Eq. (2.72), we can obtain the corresponding eigenvalue of the original system. Through the above expansions, we obtain

$$\mathcal{L}_-^{(0)} \phi_n^{(1)} = \gamma_1 \phi_n^{(0)} - \mathcal{L}_-^{(1)} \phi_n^{(0)}. \tag{2.81}$$

Projecting the system of Eq. (2.81) onto the kernel of $L_-^{(0)}$ eliminates the left-hand side contribution, and yields a matrix eigenvalue problem with γ_1 as its eigenvalue, namely

$$\mathcal{M}_1 c = \gamma_1 c, \tag{2.82}$$

where $c = (c_1, \ldots, c_N)$ and $\mathcal{M}_1$ is a tri-diagonal $N \times N$ matrix given by

$$(\mathcal{M}_1)_{m,n} = (f_m, L_-^{(1)} f_n). \tag{2.83}$$

Note that this matrix will only give non-trivial contributions if the excited sites are adjacent to each other (otherwise the relevant contributions will be vanishing). In the case of nearest-neighbor initially excited sites, based on the solution for $v_n^{(1)}$ above, the relevant matrix elements will be

$$(\mathcal{M}_1)_{n,n} = \cos(\theta_{n+1} - \theta_n) + \cos(\theta_{n-1} - \theta_n), \qquad 1 < n < N,$$

$$(\mathcal{M}_1)_{n,n+1} = (\mathcal{M}_1)_{n+1,n} = -\cos(\theta_{n+1} - \theta_n), \qquad 1 \le n < N,$$

$$(\mathcal{M}_1)_{1,1} = \cos(\theta_2 - \theta_1),$$

$$(\mathcal{M}_1)_{N,N} = \cos(\theta_N - \theta_{N-1}). \tag{2.84}$$

Equation (2.83) more generally (or e.g. the more specific Eq. (2.84) in the simplest case of adjacent site excitations), in conjunction with Eq. (2.72) allows us to obtain definitive estimates on the eigenvalues of the linearization for multisite configurations which we can subsequently directly compare with numerical results.
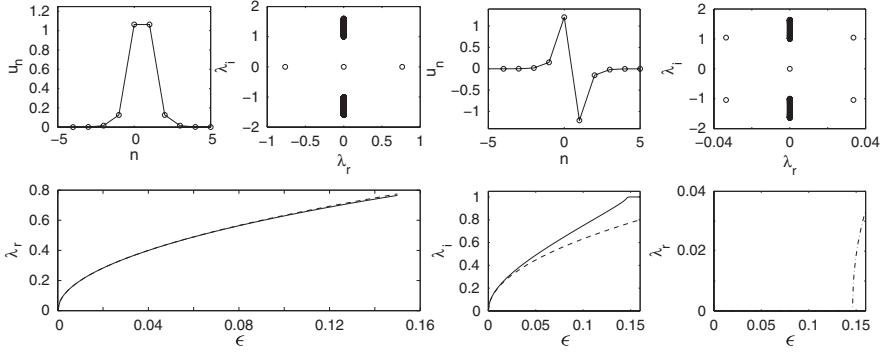
Fig. 2.9 The *top row* shows the solution profiles for the two-site in-phase mode (*first panel*) and out-of-phase mode (*third panel*) and their corresponding spectral planes (λ_r, λ_i) (*second and fourth panels*). The *bottom row* shows the relevant eigenvalue pair bifurcating from the origin. In the *left panel* it is becoming real for the in-phase mode (*solid line*: numerics, *dashed line*: theoretical prediction $\lambda = 2\sqrt{\epsilon}$). In the *right panel*, it becomes imaginary (*solid line*: numerics, *dashed line*: theoretical prediction $\lambda = 2\sqrt{\epsilon}i$). It eventually collides with the band edge of the continuous spectrum for $\epsilon > 0.146$, giving rise to a complex eigenvalue quartet (its real part is shown in the *rightmost panel*). Reprinted from [37] with permission

Such comparisons are illustrated in Fig. 2.9, for the case of two-site excitations. Fig. 2.9 presents both the case where the two excited sites are in phase (this corresponds to the unstable version of the fundamental soliton), as well as that where they are out of phase, which corresponds to the well-known example of the so-called twisted mode (see, e.g., [49–52] and references therein). In this simplest multisite case of two adjacent site excitations, the relevant matrix $\mathcal{M}_1$ becomes

$$\mathcal{M}_1 = \begin{pmatrix} \cos(\theta_1 - \theta_2) & -\cos(\theta_1 - \theta_2) \\ -\cos(\theta_1 - \theta_2) & \cos(\theta_1 - \theta_2) \end{pmatrix}, \tag{2.85}$$

whose straightforward calculation of eigenvalues leads to $\lambda^2 = 0$ (as is expected from the U(1) invariance, one eigenvalue pair should remain at zero) and $\lambda^2 = 2\epsilon \cos(\theta_1 - \theta_2)$. Note that this result is consonant with our qualitative theory above since for same phase excitations ($\theta_1 = \theta_2$), the configuration is unstable, while the opposite is true if $\theta_1 = \theta_2 \pm \pi$. The top subplots of the figure show typical mode profiles (first and third panel) and the spectral plane $\lambda = \lambda_r + i\lambda_i$ of the corresponding linear eigenvalue problem (second and fourth panel) for $\epsilon = 0.15$. The bottom subplots indicate the corresponding real (for the in-phase mode) and imaginary (for the twisted anti-phase mode) eigenvalues from the theory (dashed line) versus the full numerical result (solid line). We find the agreement between the theory and the numerical computation to be excellent in the case of the in-phase excitation. For the twisted out-of-phase excitation, the agreement is within the 5%-error for $\epsilon < 0.0258$. For larger values of ϵ, the difference between the theory and numerics grows. The imaginary eigenvalues collide at $\epsilon \approx 0.146$ with the band

edge of the continuous spectrum, such that the real part λ_r becomes non-zero for $\epsilon > 0.146$ (recall that these eigenvalues have negative Krein signature, hence, their collision with eigenvalues of the band edge of the continuous spectrum or ones bifurcating therefrom leads to complex quartets [40, 41] due to a Hamiltonian–Hopf bifurcation [53]).

In the case $N = 3$, the discrete three-pulse solitons consist of the three modes as follows:

$$\text{(a)} \quad \theta_1 = \theta_2 = \theta_3 = 0,$$
$$\text{(b)} \quad \theta_1 = \theta_2 = 0, \ \theta_3 = \pi, \tag{2.86}$$
$$\text{(c)} \quad \theta_1 = 0, \ \theta_2 = \pi, \ \theta_3 = 0.$$

The eigenvalues of matrix $\mathcal{M}_1$ are given explicitly as $\gamma_1 = 0$ and

$$\gamma_{2,3} = \cos(\theta_2 - \theta_1) + \cos(\theta_3 - \theta_2)$$
$$\pm \sqrt{\cos^2(\theta_2 - \theta_1) - \cos(\theta_2 - \theta_1)\cos(\theta_3 - \theta_2) + \cos^2(\theta_3 - \theta_2)}.$$

The in-phase mode (a), which can be symbolically denoted $+ + +$ has two real unstable eigenvalues $\lambda \approx \sqrt{6\epsilon}$ and $\sqrt{2\epsilon}$ in the stability problem for small $\epsilon > 0$. The mode (b), symbolically represented as $+ + -$, has one real unstable eigenvalue pair $\lambda \approx \pm\sqrt{2\sqrt{3}\epsilon}$ and a simple pair of purely imaginary eigenvalues $\lambda \approx \pm i\sqrt{2\sqrt{3}\epsilon}$ with negative Krein signature. This pair may bifurcate to the complex plane as a result of the Hamiltonian–Hopf bifurcation. Finally mode (c) $(+ - +)$ has no unstable eigenvalues but two pairs of purely imaginary eigenvalues $\lambda \approx \pm i\sqrt{6\epsilon}$ and $\lambda \approx \pm i\sqrt{2\epsilon}$ with negative Krein signature. The two pairs may bifurcate to the complex plane as a result of the two successive Hamiltonian–Hopf bifurcations.

Figure 2.10 summarizes the results for the three modes (a–c), given in (2.86), in a presentation similar to that of Fig. 2.9. For the in-phase mode (a), two real positive eigenvalues give rise to instability for any $\epsilon \neq 0$. The error between theoretical and numerical results is within 5% for $\epsilon < 0.15$ for one real eigenvalue and for $\epsilon < 0.0865$ for the other eigenvalue. Similar results are observed for the mode (b), where the real positive eigenvalue and a pair of imaginary eigenvalues with negative Krein signature are generated for $\epsilon > 0$. The imaginary eigenvalue collides with the band edge of the continuous spectrum at $\epsilon \approx 0.169$, which results in a complex eigenvalue quartet. Finally, in the case of the out-of-phase mode (c), two pairs of imaginary eigenvalues with negative Krein signature exist for $\epsilon > 0$ and lead to the emergence of two complex quartets of eigenvalues. The first one occurs for $\epsilon \approx 0.108$, while the second one occurs for much larger values of $\epsilon \approx 0.223$.

One can do a similar calculation for the case in which the excited sites are not adjacent to each other, but are rather, e.g., one site apart. This is detailed in [37]. In that case, some of the logistic details change, most notably that we have to get to the second-order correction $\epsilon^2\phi^{(2)}$, since the leading order correction does not
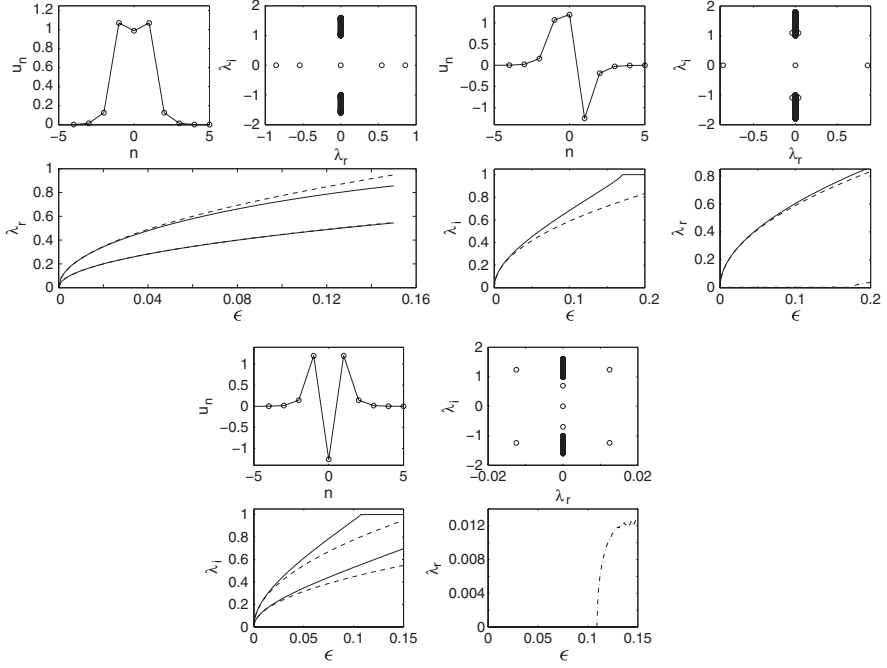
Fig. 2.10 Same as Fig. 2.9, but for the three-site branches $+++$ (*left panels*), $++-$ (*right panels*), and $+-+$ (*bottom panels*). Reprinted from [37] with permission

contribute to the excited sites. Furthermore, accordingly, the leading order in the expansion of the eigenvalue of L_- should be $\gamma = \epsilon^2 \gamma_2$. Then, the relevant perturbation equation becomes

$$L_-^{(0)} \phi_n^{(2)} = \gamma_2 \phi_n^{(0)} - L_-^{(1)} \phi_n^{(1)} - L_-^{(2)} \phi_n^{(0)}. \tag{2.87}$$

Subsequent projection to the kernel of $L_-^{(0)}$ yields an equation entirely analogous to Eq. (2.82) with the only difference that γ_1 and $\mathcal{M}_1$ are replaced by γ_2 and $\mathcal{M}_2$, with the latter being defined as per Eq. (2.84) but with the relevant angles being the next-nearest-neighbor excited ones. It is then straightforward to extract the analogous predictions as for the nearest-neighbor sites, but now the relevant eigenvalues, while having the same prefactors, they will be $\propto \epsilon$, rather than to $\sqrt{\epsilon}$. Note that this feature can be appropriately generalized for excitations that are k sites apart. These will "cross-talk" to each other at the kth order (and above), and the corresponding eigenvalues bifurcating from the origin will be to leading order $O(\epsilon^{k/2})$ (or higher).

The corresponding numerical results are shown in Fig. 2.11 for two sites and Fig. 2.12 for three sites, which are entirely analogous to Figs. 2.9 and 2.10, respectively. In the in-phase, two-site case, the agreement with the theory is excellent for $\epsilon < 0.2$. For the twisted mode, we also have very good agreement for $\epsilon < 0.415$;
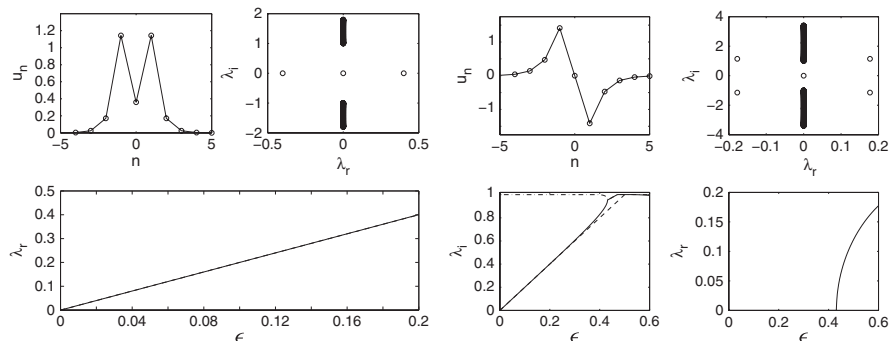
Fig. 2.11 A direct analog to Fig. 2.9, but now for the case of next-nearest-neighbor two-site excitations. The resulting eigenvalues are (approximately) linear in ϵ in this case. Reprinted from [37] with permission
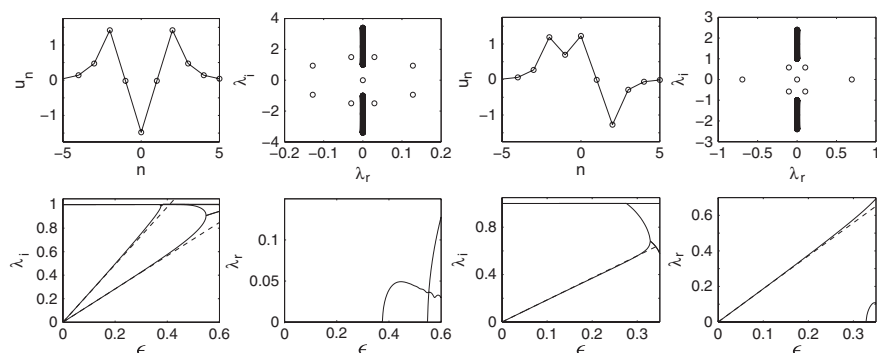

Fig. 2.12 A direct analog to Fig. 2.10, but now for the case of next-nearest-neighbor three-site excitations. The resulting eigenvalues are (approximately) linear in ϵ in this case. Reprinted from [37] with permission

the Hamiltonian–Hopf bifurcation occurs at $\epsilon \approx 0.431$ (in this case, the collision occurs with an eigenvalue that has bifurcated from the band edge of the continuous spectrum). Similarly, for the three-site excitations, we observe excellent agreement in the examined range between the numerical results and the corresponding theoretical predictions. Here, the quartets emerge at $\epsilon \approx 0.328$ for the $+ + -$ mode, while for $+ - +$, there are two such bifurcations arising at $\epsilon \approx 0.375$ and 0.548, respectively.

2.2.2 A Different Approach: Perturbed Hamiltonian Systems

We now take a detour to provide a different (and more general) approach to the stability problem of the one-dimensional DNLS system, while discussing some

recent general results for this class of systems developed in [54, 55, 57]. These recent results were obtained on the basis of Lyapunov–Schmidt reductions, as well as through the earlier, important functional analytic work of [28, 42].

Our starting point will be a perturbed system of the general form

$$\frac{du}{dt} = J E'(u), \tag{2.88}$$

where J is the usual invertible skew-symmetric operator with bounded inverse and $E(u) = E_0(u) + \epsilon E_1(u)$, with $0 < \epsilon << 1$. Here $E(u)$ represents the total energy of the system. The underlying assumption is that the perturbation breaks some of the symmetries of the unperturbed problem. The aim of these results is to relate the spectrum (denoted henceforth by σ) $\sigma(E''(\Phi))$ to $\sigma(J E''(\Phi))$, where Φ represents a solution to the steady-state problem $E'(u) = 0$. The operator $E''(\Phi)$ is self-adjoint; hence, $\sigma(E''(\Phi)) \subset \mathbb{R}$. Since $J E''(\Phi)$ is the composition of a skew-symmetric operator with a self-adjoint operator, if $\lambda \in \sigma(J E''(\Phi))$, then $-\lambda, \pm\lambda^* \in \sigma(J E''(\Phi))$. Thus, eigenvalues for $J E''(\Phi)$ come in quartets. Below one sees the manner in which the negative directions for $E''(\Phi)$ influence the unstable spectrum of $J E''(\Phi)$. It is of particular relevance to note that negative directions for $E''(\Phi)$ do *not* necessarily lead to an exponential instability of the wave. A detailed discussion of the proof of these results can be found in [55]. The more epigrammatic discussion of these results below follows the work of [57].

2.2.2.1   The Unperturbed Problem

Let H be a Hilbert space with inner product $\langle \cdot, \cdot \rangle$; also denote by G a finite-dimensional Abelian connected Lie group with Lie algebra $\mathfrak{g}$, setting $\dim(\mathfrak{g}) = n$. We use $e^{\omega} := \exp(\omega)$ to denote the exponential map from $\mathfrak{g}$ to G. Let T be a unitary representation of G on H, so that $T'(e)$ maps $\mathfrak{g}$ into the space of closed skew-symmetric operators. Denote $T_{\omega} := T'(e)\omega$ as the generator of the semigroup $T(e^{\omega t})$, and note that T_{ω} is linear in $\omega \in \mathfrak{g}$. The group orbit Gu is defined by $Gu := \{T(g)u : g \in G\}$. It is assumed that E is invariant under a group orbit, i.e., $E(T(g)u) = E(u)$ for all $g \in G$ and $u \in H$. Define the functional $Q_{\omega}(u) := \frac{1}{2}\langle J^{-1}T_{\omega}u, u \rangle$, and note that $Q''_{\omega} = J^{-1}T_{\omega}$ is a symmetric linear operator. Furthermore, Q_{ω} is invariant under a group orbit.

The Hamiltonian system of interest is given by

$$\frac{dv}{dt} = J E'(v).$$

We are interested in relative equilibria of this system, i.e., stationary solutions which satisfy $u(t) \in Gu(0)$ for all t. A relative equilibrium satisfies $u(t) = T(e^{\omega t})u(0)$ for some $\omega \in \mathfrak{g}$. Changing variables via

$$v(t) = T(\exp(\omega t))u(t),$$

leads to the system

$$\frac{du}{dt} = J E_0'(u; \omega), \qquad (2.89)$$

where

$$E_0'(u; \omega) := E'(u) - J^{-1} T_\omega u.$$

We are therefore seeking critical points of the functional $E_0(u; \omega) := E(u) - Q_\omega(u)$ for some $\omega \in \mathfrak{g}$.

The steady-state equation is

$$E_0'(u; \omega) = 0$$

and we assume that it has a smooth family $\Phi(\omega)$ of solutions, where ω varies in $\mathfrak{g}$. Furthermore, we assume that the isotropy subgroups $\{g \in G : T(g)\Phi(\omega) = \Phi(\omega)\}$ are discrete. This assumption implies that the group orbits $G\Phi(\omega)$ have dimension n for each fixed $\omega \in \mathfrak{g}$. Since G is Abelian, for each fixed $\omega \in \mathfrak{g}$ the entire group orbit $T(g)\Phi(\omega)$ consists of relative equilibria with time evolution $T(e^{\omega t})$.

We denote the linearization operator around the wave by $J E_0''$. Fix a basis $\{\omega_1, \ldots, \omega_n\}$ that satisfies the property that the set $\{T_{\omega_1}\Phi, \ldots, T_{\omega_n}\Phi\}$ is orthogonal. One has that $E_0'' T_{\omega_j}\Phi = 0$ for $j = 1, \ldots, n$; see Section 2 of [55]. Since G is Abelian, under the non-degeneracy condition that D_0 is non-singular, where D_0 is defined in (2.91), it is known that the operator $J E_0''$ will have a non-trivial kernel

$$J E_0''(\Phi) T_{\omega_i}\Phi = 0, \qquad J E_0''(\Phi)\partial_{\omega_i}\Phi = T_{\omega_i}\Phi \qquad (2.90)$$

for $i = 1, \ldots, n$, with $\partial_\omega := \partial/\partial\omega$. Furthermore, this set is a basis for the kernel. Note that solutions to the above linear system yield not only a basis for the tangent space to the group orbit, but also a basis for the tangent space of the manifold of relative equilibria. We will assume that the linear operator E_0'' is Fredholm of index zero. If one sets

$$Z = \mathrm{Span}\{T_{\omega_1}\Phi, \ldots, T_{\omega_n}\Phi\},$$

then $H = N \oplus Z \oplus P$, where N is the finite-dimensional subspace

$$N = \{u \in H : \langle u, E_0'' u \rangle < 0\}$$

and $P \subset H$ is a closed subspace such that

$$\langle u, E_0'' u \rangle > \delta \langle u, u \rangle, \quad u \in P$$

for some constant $\delta > 0$.

We set

$$H_1 := \{u \in H \; : \; \langle u, E_0'' \partial_{\omega_i} \Phi \rangle = 0, \; i = 1, \dots, n\}.$$

It is shown in [58] that when solving the linear eigenvalue problem $J E_0''(\Phi)u = \lambda u$, it is sufficient to consider only those $u \in H_1$. This also follows from standard solvability theory, as $J^{-1} T_{\omega_i} \Phi = E_0'' \partial_{\omega_i} \Phi$ are solutions to the adjoint eigenvalue problem at $\lambda = 0$ for $i = 1, \dots, n$. We now define the symmetric matrix $D_0 \in \mathbb{R}^{n \times n}$ by

$$(D_0)_{ij} = \langle \partial_{\omega_j} \Phi, E_0'' \partial_{\omega_i} \Phi \rangle. \tag{2.91}$$

For a given self-adjoint operator A, we denote the number of negative eigenvalues by n(A), while p(A) will be the number of positive eigenvalues, and z(A) the number of zero eigenvalues.

The following was proved in [8]. Suppose that z(D_0) = 0. The operator E_0'' restricted to the space H_1 has the negative index

$$\mathrm{n}\left(E_0''|_{H_1}\right) = \mathrm{n}\left(E_0''\right) - \mathrm{n}(D_0).$$

If n($E_0''|_{H_1}$) = 0, then the wave is a local minimizer for the energy $E_0(u)$, and is therefore stable. The interpretation of this statement can be made as follows. Suppose that the operator E_0'' satisfies n(E_0'') = $k \geq 1$. One then has that the wave is not a local minimizer for E_0. However, there are conserved quantities associated with the evolution equation, and it is possible that these quantities may "prohibit" accessing some or all of the unstable eigendirections. The dim($\mathfrak{g}$) conserved quantities are given by

$$Q_i(u) := \frac{1}{2} \langle J^{-1} T_{\omega_i} u, u \rangle, \quad i = 1, \dots, n.$$

The quantity n(D_0) precisely determines the number of directions which are rendered inaccessible by the conserved quantities. Hence, n(E_0'')−n(D_0) determines the number of unstable directions for the energy after the constraints have been taken into account.

2.2.2.2 The Perturbed Problem

We now turn to the perturbed problem, where the energy is of the form $E_0(u) + \epsilon E_1(u)$, with $0 < \epsilon \ll 1$. It is assumed that the perturbation breaks $1 \leq k_s \leq n$ of the original symmetries, so that the perturbed system will have $n - k_s$ symmetries. Furthermore, it is assumed that the problem is well-understood for $\epsilon = 0$, as per the above discussion. The existence question is settled by the work of [54], through the following condition, based on Lyapunov–Schmidt reductions: a necessary condition for persistence of the wave is

$$\langle E_1'(\Phi(\omega)), T_{\omega_j}\Phi\rangle = 0, \quad j = 1, \ldots, n \tag{2.92}$$

for some $\omega \in \mathfrak{g}$. The condition is sufficient if $z(M) = n - k_s$, where the symmetric matrix M satisfies

$$M_{ij} := \langle T_{\omega_i}\Phi, E_1''(\Phi(\omega)) T_{\omega_j}\Phi\rangle.$$

Since the perturbation breaks k_s symmetries, and the system is Hamiltonian, $2k_s$ eigenvalues will leave the origin. The following lemma, which tracks these small eigenvalues, was proven in [55] via a Lyapunov–Schmidt reduction: the $O(\sqrt{\epsilon})$ eigenvalues and associated eigenfunctions for the perturbed problem are given by

$$\lambda = \sqrt{\epsilon}\,\lambda_1 + O(\epsilon), \quad u = \sum_{i=1}^{n} v_i \left(T_{\omega_i}\Phi + \sqrt{\epsilon}\,\lambda_1 \partial_{\omega_i}\Phi\right) + O(\epsilon),$$

where λ_1 is the eigenvalue and $\mathbf{v}$ is the associated eigenvector for the generalized eigenvalue problem

$$\left(D_0\lambda_1^2 + M\right)\mathbf{v} = \mathbf{0}.$$

It should be noted that the above eigenvalue problem will have $2(n - k_s)$ zero eigenvalues, due to the fact that this many symmetries are assumed to be preserved under the perturbation.

If an eigenvalue has non-zero real part, the Krein signature is zero [46, 59]. The Krein signature of a purely imaginary $O(\sqrt{\epsilon})$ eigenvalue given above is

$$K = \text{sign}\left(\mathbf{v}^T M \mathbf{v}\right) = \text{sign}(\mathbf{v}^T D_0 \mathbf{v}), \tag{2.93}$$

where $\mathbf{v}$ is the associated eigenvector [55]. It may also be possible for eigenvalues to emerge out of the continuous spectrum, creating internal modes, as discussed above. Since these eigenvalues will be of $O(1)$, they will not be captured by the perturbation expansion given in the above lemma. However, this is not problematic (at least in models of the DNLS type) since any $O(1)$ eigenvalues will be purely imaginary with positive Krein sign, and hence for small ϵ do not contribute to an instability.

In the statement of the theorem below, the symmetric matrix D_ϵ is defined by

$$(D_\epsilon)_{ij} := \mathbf{w}_i^T D_0 \mathbf{w}_j, \tag{2.94}$$

where the set $\{\mathbf{w}_1, \ldots, \mathbf{w}_{n-k_s}\}$ is a basis for $\ker(M)$. The following is proved in [55] regarding $\sigma(J(E_0'' + \epsilon E_1''))$ for $0 < \epsilon \ll 1$.

Theorem 1. *Suppose that the unperturbed wave is stable, i.e., $n(E_0'') = n(D_0)$. Let k_r represent the number of real negative eigenvalues, $2k_c$ the number of complex eigenvalues with negative real part, and $2k_i$ the number of purely imaginary eigenvalues with negative Krein signature for the perturbed problem (counting multiplicity). Assume that $z(D_\epsilon) = 0$. Then*

$$k_r + 2k_c + 2k_i = n(E_0'') + n(M) - n(D_\epsilon). \tag{2.95}$$

Furthermore, all of these eigenvalues are of $O(\sqrt{\epsilon})$, *and*

$$k_s \geq k_r \geq |n(M) - (n(D_0) - n(D_\epsilon))|.$$

Any eigenvalues arising from an edge bifurcation will be purely imaginary with positive Krein signature.

The following remarks can be made about the count of eigenvalues:

1. The upper bound on k_r arises from the facts that there are only $2k_s$ eigenvalues of $O(\sqrt{\epsilon})$ and the system is Hamiltonian.
2. Since $n(D_\epsilon) \leq n(D_0) = n(E_0'')$, the perturbed wave cannot be a minimizer unless $n(M) = 0$ and that $n(D_\epsilon) = n(D_0)$.

One possible interpretation of 1 is as follows. As previously mentioned, for the unperturbed problem each unstable direction associated with E_0'' is neutralized by an invariance, which in turn are each generated by a symmetry. Now, D_ϵ is the representation of D_0 when restricted to the symmetry group which persists upon the perturbation. The quantity

$$n(E_0'') - n(D_\epsilon) = n(D_0) - n(D_\epsilon)$$

then precisely details the number of unstable directions associated with E_0'' which are no longer neutralized by the invariances. The quantity $n(M)$ is the number of additional unstable directions generated by the symmetry-breaking perturbation E_1. The theorem essentially illustrates that the number of potentially unstable eigenvalue pairs in the system is obtained by keeping track of these eigendirections.

2.2.2.3 Case Example: DNLS from the Anti-Continuum Limit

One can consider the DNLS equation near the AC limit as such a perturbed problem. In fact, one can do this even for a general interaction matrix between sites (that is not restricted to nearest-neighbor interactions) as follows:

$$i\dot{u}_n + u_n - |u_n|^2 u_n = -\epsilon \sum_{m=1}^{N} k_{nm} u_m. \tag{2.96}$$

Then, one can label the unperturbed energy at the AC limit as

$$E_0(u) = \sum_n |u_n|^2 - \frac{1}{2}|u_n|^4, \tag{2.97}$$

while the relevant perturbation will be of the form

$$E_1(u) = -\epsilon \sum_{n,m=1}^{N} k_{nm} \left(u_n^\star u_m + u_n u_m^\star \right). \tag{2.98}$$

At the AC limit, the solutions for the excited sites will be $u_n = e^{i\theta_n}$, where the θ_n are free arbitrary phase parameters.

To determine the persistence of the waves, one has to evaluate the perturbed energy at the unperturbed limit solution, in which case, we can straightforwardly evaluate it to be

$$E_1 = - \sum_{n,m=1}^{N} 2k_{nm} \cos(\theta_n - \theta_m). \tag{2.99}$$

Based on the discussion of the previous subsection, the persistence conditions then read $\partial_{\theta_n} E_1 = 0$, which leads to an equivalent condition as Eq. (2.60) derived previously, namely

$$\sum_{m \neq n} k_{nm} \sin(\theta_n - \theta_m) = 0. \tag{2.100}$$

One can subsequently based on the above theory evaluate the relevant matrices D_0 and M_{ij} that enter the stability calculation, in order to obtain information for the relevant eigenvalues that will leave the origin of the spectral plane, upon deviation from the AC limit of $\epsilon = 0$. One can thus find that

$$D_0 = -I_N, \tag{2.101}$$
$$M_{ij} = \partial^2_{\theta_i \theta_j} E_1. \tag{2.102}$$

I_N is the unit matrix of size N (the number of excited sites). Then the correction λ_1 to the eigenvalues will be obtained from the reduced eigenvalue problem $(D_0 \lambda_1^2 + M)v = 0$ which leads in our case to

$$\left(-I_N \lambda_1^2 + 2\mathcal{M}_1 \right) v = 0, \tag{2.103}$$

since $M = 2\mathcal{M}_1$, where $\mathcal{M}_1$ is defined by the Eq. (2.84) above (in the nearest-neighbor case; in fact the result obtained here is also true for a more general interaction matrix). This confirms the validity of the direct calculation given above, but also places these results in a broader context of perturbed Hamiltonian dynamics.

Before closing this subsection, we should also note that the eigenvalue count given above confirms the closure relation of [55] (see also [60]), since $n(E_0'') = N + m$ (where N is the number of excited sites and m the number of sign changes between them), $k_r = N - m - 1$, $k_c = 0$, and $k_i = m$, with the imaginary eigenvalues bearing negative Krein signature. A direct calculation shows that $n(M) - n(D_\epsilon) = -1$ and therefore the relevant relation is satisfied.

2.2.3 Multipulses Close to the Continuum Limit

We close the discussion of the one-dimensional problem by briefly considering the case of multipulses in the vicinity of the continuum limit, following closely the discussion of [39] (for this reason, we also use $\epsilon = 1/(2h^2)$, with $h \to 0$ and $\beta = -1$ in Eq. (2.1)). In the quasi-continuum approximation, it can be obtained that the interaction between two solitons is given by the potential energy

$$U_{int}(\xi_i - \xi_2, \Delta\phi) = -8\eta^3 \exp(-\eta|\xi_1 - \xi_2|) \cos(\Delta\phi). \qquad (2.104)$$

In this expression $\Delta\xi = \xi_1 - \xi_2$ is the relative separation between the wave centers and $\Delta\phi$ is the relative phase which also plays an important role in their interaction. In particular, note that the interaction is *attractive* for in-phase solitons, while exactly the opposite (i.e., repulsion) is true for out-of-phase solitary waves. Although this result can be derived using the perturbation technique of Karpman and Solov'ev [61] or the variational approximation [34], here we present a different and fairly direct approach of obtaining it, due to Manton [63] (who pioneered it in Klein–Gordon-type equations). Here, we are following the relevant discussion of [64].

In the case of the NLS equation, we have defined previously the mass (whose role is played by the squared L^2 norm, given by Eq. (2.6), while the momentum is defined in Eq. (2.7) (although, in the present setting a factor of 1/2 would be multiplying the right-hand side). Assuming then that we have a soliton centered at $\xi = 0$ and one at $\xi = \Delta\xi$, we can find the derivative of the momentum (the "force") evaluated between $a \ll 0$ and $0 \ll b \ll \Delta\xi$. (This brings in the assumption of sufficiently large separation between the waves for this approach to work.) We thus obtain

$$\frac{dM}{dt} = \frac{1}{4} \left[uu_{xx}^\star + u_{xx}u^\star - 2|u_x|^2 \right]_a^b. \qquad (2.105)$$

Note that if integrating between $-\infty$ and ∞, Eq. (2.105) would yield a vanishing right-hand side, due to the total conservation of the momentum. However, in the present setting, it yields a non-vanishing contribution to the solitary wave in this interval (a non-vanishing force) due to the solitary wave outside of the interval. Hence, we can use this approach to infer the force exerted from one soliton to the other (and also their respective equations of motion). We use the standard two-soliton decomposition, $u = u^{(1)} + u^{(2)}$ where $u^{(1)} = \eta\,\mathrm{sech}(\eta x)\exp(i\eta^2 t/2)$, $u^{(2)} = \eta\,\mathrm{sech}(\eta(x - \Delta\xi))\exp(i\eta^2 t/2)\exp(i\phi)$ are the standing waves, and the relative phase ϕ between them has been incorporated in u_2. Then, one obtains

$$\frac{dM}{dt} = 8\eta^4 \exp(-\eta\Delta\xi), \qquad (2.106)$$

which results in the dynamical equation for the separation (using the mass of the soliton; see also the details of the discussion of [64]) of the form

$$\ddot{\Delta\xi} = -8\eta^3 \exp(-\eta\Delta\xi)\cos\phi.$$ (2.107)

The anti-derivative of the right-hand side of Eq. (2.106) yields the potential of interaction between the solitary waves, coinciding with the result of Eq. (2.104).

In the continuum, this interaction does not allow for the formation of (stationary) bound states between the solitary waves. However, in the realm of the lattice (near the continuum limit), the idea of [39] was that each of the solitary waves will face the energetic contributions of two distinct factors: on the one hand, there will be the interaction with the second solitary wave. On the other hand, each of the waves will be subject to the PN potential due to the existence of the lattice. The latter energetic contribution has been described previously. An asymptotic lowest order approximation of the relevant formula was used in [39] in the form

$$H_{PN}(\xi) \approx -\frac{8\pi^4}{3h^3} \exp\left(-\frac{\pi^2}{\eta h}\right)\cos\left(\frac{2\pi}{h}\xi\right).$$ (2.108)

Then, the full energy landscape can be described as

$$H \approx H_{PN}(\xi_1) + H_{PN}(\xi_2) + U_{int}(\xi_1 - \xi_2, \Delta\phi)$$ (2.109)

and it is expected that the locations of the centers of the relevant solitary waves can be obtained from extremization of the energy of Eq. (2.109).

While the expression of Eq. (2.109) gives a nice intuitive way to understand the balance of interactions for multipulses in the lattice setting (see also the relevant sketch of Fig. 2.13), for practical purposes, it is perhaps less useful. This is because if h is small, the H_{PN} terms are exponentially weak and hence are practically negligible in comparison to the interaction energy, while for h large so that these terms are sizeable, the pulse deviates from its continuous form and the calculation of H_{PN} is less accurate based on the quasi-continuum expression. Hence, given the nature of the approximations in the calculation, we do not attempt to test it quantitatively herein, although we acknowledge its qualitative usefulness in elucidating the relevant energy landscape (see also the relevant discussions in [65]).

It is interesting to compare/contrast this picture with the integrable analog of the DNLS, namely the AL-NLS model, where the above-mentioned Manton calculation can be carried through [66]. In the latter case, as discussed in the beginning of the chapter, the conserved momentum is given by Eq. (2.25). As in the continuum case, we now consider two solitons, one centered at 0 and one centered at $s \gg 0$, i.e., *widely separated*. We compute dM/dt by performing the summation over n not for the infinite lattice (when the result would be zero due to the relevant conservation law), but rather from $n = L$ to $n = N$, with $L \ll 0$, and $0 \ll N \ll \Delta\xi$. The idea behind this calculation is that, in fact, the force in this interval is not going to be zero, but rather would be *finite* due to the soliton–soliton interaction. For a finite interval encompassing only one soliton, the amount of momentum gain is finite, due to the fact that the one soliton experiences the pull (or push) of the other soliton at
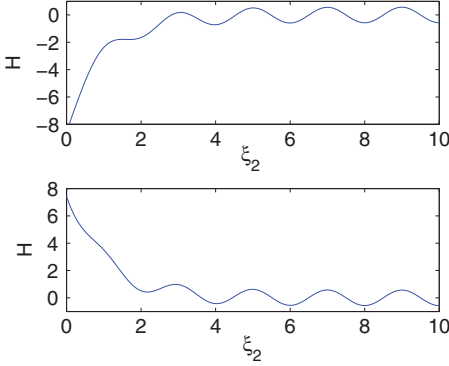
Fig. 2.13 The energy landscape of Eq. (2.109), as it is given for the interaction of two identical solitary waves with $\eta = 1$, for $h = 2$. The first wave is located at $\xi_1 = 0$ and the contributions to the energy landscape affecting the second solitary wave are shown as a function of its center location ξ_2. The *top panel* shows the case of attractive interaction for $\Delta\phi = 0$, while the *bottom panel* shows the case of repulsive interaction for $\Delta\phi = \pi$

the boundary of the interval where we perform the calculation. Specifically, we can evaluate

$$
\begin{aligned}
\frac{dM}{dt} = & -2 \sum_{n=L}^{N} \left(|u_{n+1}|^2 - |u_n|^2 \right) \\
& + \sum_{n=L}^{N} \left(u_n u_{n+2}^\star + u_n^\star u_{n+2} \right) \left(1 + |u_{n+1}|^2 \right) \\
& - \sum_{n=L}^{N} \left(u_{n-1} u_{n+1}^\star + u_{n-1}^\star u_{n+1} \right) \left(1 + |u_n|^2 \right) .
\end{aligned}
\tag{2.110}
$$

However, observing the telescopic nature of the sums in the right-hand side of Eq. (2.110), we infer that

$$
\begin{aligned}
\frac{dM}{dt} = & -2 \left(|u_{N+1}|^2 - |u_L|^2 \right) \\
& + \left(u_N u_{N+2}^\star + u_N^\star u_{N+2} \right) \left(1 + |u_{N+1}|^2 \right) \\
& - \left(u_{L-1} u_{L+1}^\star + u_{L-1}^\star u_{L+1} \right) \left(1 + |u_L|^2 \right) .
\end{aligned}
\tag{2.111}
$$

As usual in Manton's method, and based on intuitive physical arguments, the main contribution in this asymptotic calculation stems from the boundary between the two solitons. Hence, we drop the terms with subscript L and only consider the contributions with subscript N in what follows.

We then select a two-soliton ansatz

$$u_n = u_n^{(1)} + u_n^{(2)} \tag{2.112}$$

with $u_n^{(1)} = \sinh(\gamma)\mathrm{sech}(\gamma n)\exp(i\sigma)$ and $u_n^{(2)} = \sinh(\gamma)\mathrm{sech}(\gamma(n-\Delta\xi))\exp(i\sigma)$ (i.e., two in-phase solitons). Since $0 \ll N \ll \Delta\xi$, we can use the asymptotic form of the soliton tail at $n = N$, according to

$$u_n^{(1)} = 2\sinh(\gamma)\exp(-\gamma N)\exp(i\sigma), \tag{2.113}$$

$$u_n^{(2)} = 2\sinh(\gamma)\exp(\gamma(N-\Delta\xi))\exp(i\sigma). \tag{2.114}$$

Through direct substitution of Eq. (2.112) and the expressions in Eqs. (2.113) and (2.114) into Eq. (2.111), we obtain that

$$\frac{dM}{dt} \approx 32\sinh^4(\gamma)\exp(-\gamma\Delta\xi). \tag{2.115}$$

Using Newton's equation of motion for the solitons we obtain

$$P_s\ddot{\Delta\xi} = -2\frac{dM}{dt}, \tag{2.116}$$

where M_s is the mass (power) of the soliton; the factor "2" comes from the fact that there is an equal and opposite pull (or push) on the second soliton, and hence their relative distance decreases by twice the contribution of dM/dt to each of them; and finally the "−" sign originates from the fact that a positive boundary contribution to dM/dt decreases the soliton distance, while the opposite is true for a negative dM/dt. In this case,

$$P_s = \sum_{n=-\infty}^{\infty} \ln\left(1 + |\psi_n|^2\right) = 2\gamma. \tag{2.117}$$

Thus, the equation for the $s(t)$ becomes

$$\ddot{\Delta\xi} = -\frac{32}{\gamma}\sinh^4(\gamma)\exp(-\gamma\Delta\xi), \tag{2.118}$$

while the relevant effective soliton interaction potential (for a unit mass particle) is

$$V(\Delta\xi) = -\frac{32}{\gamma^2}\sinh^4(\gamma)\exp(-\gamma\Delta\xi). \tag{2.119}$$

If the solitons additionally possess a phase difference ϕ, the above calculations gives a factor of $\cos(\phi)$ in Eqs. (2.118) and (2.119). Relevant results illustrating the attraction of in-phase and repulsion of out-of-phase solitons are shown in Fig. 2.14.
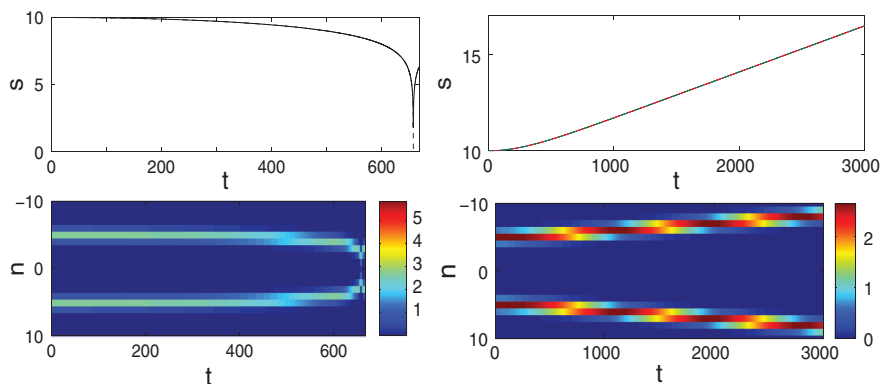
Fig. 2.14 Example of an in-phase (*left*) and an out-of-phase (*right*) collision of two discrete bright solitons of the AL-NLS model. The *top panels* show the distance $s(t) \equiv \Delta \xi$ numerically and from the ODE of Eq. (2.118), while the *bottom* shows the space-time contour plot of the AL-NLS evolution. The quality of the agreement of the ODE result with the full numerical computation is such that the two lines of the *top panels* can not be distinguished. Reprinted from [66] with permission

It should be pointed out that, as expected, the AL-NLS solitons do *not* face a PN barrier when traveling through the lattice. For this reason, the only contribution to their potential energy stems from the exponential tail–tail interactions, contrary to what we saw is the case in the DNLS model. Finally, accounting for a factor of 1/2 in the equation (and also another such factor in the definition of the momentum), as well as taking the limit of $\sinh(\gamma) \to \gamma$, we can derive the continuum analog (2.107) of Eq. (2.118).

References

1. Sulem, C., Sulem, P.L.: The Nonlinear Schrödinger Equation. Springer-Verlag, New York, (1999)
2. Morrison, P.J.: Rev. Mod. Phys. **70**, 467–521 (1998)
3. Ablowitz, M.J., Segur, H.: Solitons and the Inverse Scattering Transform. SIAM, Philadelphia (1981)
4. Kaup, D.J.: Phys. Rev. A **42**, 5689 (1990)
5. Johansson, M., Aubry, S.: Phys. Rev. E **61**, 5864 (2000)
6. Ablowitz, M.J., Ladik, J.F.: J. Math. Phys. **16**, 598 (1975)
7. Ablowitz, M.J., Ladik, J.F.: J. Math. Phys. **17**, 1011 (1976)
8. Ablowitz, M.J., Prinari, B., Trubatch, A.D.: Discrete and Continuous Nonlinear Schrödinger Systems. Cambridge University Press, Cambridge (2004)
9. Sievers, A.J., Takeno, S.: Phys. Rev. Lett. **61**, 970 (1988)
10. Page, J.B.: Phys. Rev. B **41**, 7835 (1990)
11. Kivshar, Yu.S., Campbell, D.K.: Phys. Rev. E **48**, 3077 (1993)
12. Kevrekidis, P.G., Kivshar, Yu.S., Kovalev, A.S.: Phys. Rev. E **67**, 046604 (2003)
13. Cai, D. Bishop, A.R., Grønbech-Jensen, N.: Phys. Rev. E **53**, 4131 (1996)
14. Morse, P.M., Feshbach, H.: Methods of Theoretical Physics. McGraw-Hill, New York (1953)

15. Peierls, R.F.: Proc. R. Soc. London **52**, 34 (1940)
16. Nabarro, F.R.N.: Proc. R. Soc. London **59**, 256 (1947)
17. Kivshar, Yu.S., Pelinovsky, D.E., Cretegny, T., Peyrard, M.: Phys. Rev. Lett. **80**, 5032 (1998)
18. Kapitula, T., Kevrekidis, P.G.: Nonlinearity **14**, 533 (2001)
19. Ablowitz, M.J., Herbst, B.M.: In: Important Developments in Soliton Theory, Fokas, A., Za-kharov, V. (eds.) Springer-Verlag, Berlin (1993)
20. Herbst, B.M., Ablowitz, M.J.: J. Comp. Phys. **105**, 122 (1993)
21. Kapitula, T.: SIAM J. Math. Anal. **30**, 273 (1999)
22. Kapitula, T., Rubin, J.: Nonlinearity, **13**, 77 (2000)
23. Kapitula, T., Sandstede, B.: Physica **124D**, 58 (1998)
24. Braun, O.M., Kivshar, Yu.S., Peyrard, M.: Phys. Rev. E **56**, 6050 (1997)
25. Balmforth, N.J., Craster, R.V., Kevrekidis, P.G.: Physica **135D**, 212 (2000)
26. Kevrekidis, P.G., Jones, C.K.R.T.: Phys. Rev. E **61**, 3116 (2000)
27. Kapitula, T., Kevrekidis, P.G., Jones, C.K.R.T.: Phys. Rev. E, **63** 036602 (2001)
28. Grillakis, M., Shatah, J., Strauss W.: J. Funct. Anal. **74**, 160 (1987)
29. Jones, C.K.R.T.: Ergod. Theor. Dynam. Syst. **8**, 119 (1988)
30. MacKay, R.S., Aubry, S.: Nonlinearity **7**, 1623 (1994)
31. Alfimov, G.L., Brazhnyi, V.A., Konotop, V.V.: Physica D **194**, 127 (2004)
32. Malomed, B.A., Weinstein, M.I.: Phys. Lett. A **220** 91 (1996)
33. Cuevas, J., Kevrekidis, P.G., Frantzeskakis, D.J., Malomed, B.A.: Physica D **238**, 67 (2009)
34. Malomed, B.A.: Progr. Opt. **43**, 71 (2002)
35. Kaup, D.J., Vogel, T.K.: Phys. Lett. A **362** 289 (2007)
36. Levy, H., Lessman, F.: Finite DIfference Equations, Dover, New York (1992)
37. Pelinovsky, D.E., Kevrekidis, P.G., Frantzeskakis, D.J.: Physica D **212**, 1 (2005)
38. Kevrekidis, P.G., Rasmussen, K.Ø., Bishop, A.R.: Int. J. Mod. Phys. B **15**, 2833 (2001)
39. Kapitula, T., Kevrekidis, P.G., Malomed, B.A.: Phys. Rev. E **63**, 036604 (2001)
40. MacKay, R.S., Stability of equilibria of Hamiltonian systems. In: MacKay, R.S., Meiss, J. (eds.) Hamiltonian Dynamical Systems, Adam Hilger, London (1987)
41. MacKay, R.S.: Phys. Lett. A **155**, 266 (1991)
42. Grillakis, M.: Commun. Pure Appl. Math. **43**, 299 (1990)
43. Grillakis, M.: Commun. Pure Appl. Math. **41**, 745 (1988)
44. Li, Y., Promislow, K.: Physica D **124**, 137 (1998)
45. Li, Y., Promislow, K.: SIAM J. Math. Anal. **31**, 1351(2000)
46. Skryabin, D.V.: Phys. Rev. E **64**, 055601(R) (2001)
47. Skryabin, D.V.: Phys. Rev. A **63**, 013602 (2001)
48. Kawaguchi, Y., Ohmi, T.: Phys. Rev. A **70**,043610 (2004)
49. Laedke, E.W., Kluth, O., Spatschek, K.H.: Phys. Rev. E **54**, 4299 (1996)
50. Johansson, M., Aubry, S.: Nonlinearity **10**, 1151(1997)
51. Darmanyan, S., Kobyakov, A., Lederer, F.: Sov. Phys. JETP **86**, 682 (1998)
52. Kevrekidis, P.G., Bishop, A.R., Rasmussen, K.Ø.: Phys. Rev. E **63**, 036603 (2001)
53. van der Meer, J.-C.: Nonlinearity **3**, 1041 (1990)
54. Kapitula, T.: Physica D **156**, 186 (2001)
55. Kapitula, T., Kevrekidis, P.G., Sandstede, B.: Physica D **195**, 263 (2004)
56. Kapitula, T., Kevrekidis, P.G., Sandstede, B.: Physica D **201**, 199 (2005)
57. Kapitula, T., Kevrekidis, P.G.: J. Phys. A **37**, 7509 (2004)
58. Grillakis, M., Shatah, J., Strauss, W.: J. Func. Anal. **94**, 308 (1990)
59. Aubry, S.: Physica **103D**, 201 (1997)
60. Pelinovsky, D.E.: Proc. Roy. Soc. Lond. A **461**, 783 (2005)
61. Karpman, V.I., Solov'ev, V.V.: Physica D **3**, 142 (1981)
62. Karpman, V.I., Solov'ev, V.V.: Physica D **3**, 487 (1981)
63. Manton, N.S.: Nucl. Phys. B **150**, 397 (1979)
64. Kevrekidis, P.G., Khare, A., Saxena, A.: Phys. Rev. E **70**, 057603 (2004)
65. Kevrekidis, P.G., Phys. Rev. E **64**, 026611 (2001)
66. Kevrekidis, P.G., Khare, A., Saxena, A., Bena, I.: Math. Comp. Simul. **74**, 405 (2007)